MICROGRAVITY FLOW REGIME TRANSITION MODELING

A Thesis

by

ADAM MICHAEL SHEPHARD

Submitted to the Office of Graduate Studies of
Texas A&M University
in partial fulfillment of the requirements for the degree of

MASTER OF SCIENCE

May 2009

Major Subject: Nuclear Engineering

MICROGRAVITY FLOW REGIME TRANSITION MODELING

A Thesis

by

ADAM MICHAEL SHEPHARD

Submitted to the Office of Graduate Studies of
Texas A&M University
in partial fulfillment of the requirements for the degree of

MASTER OF SCIENCE

Approved by:

Chair of Committee,	Frederick R. Best
Committee Members,	Karen Vierow
	Debjyoti Banerjee
Head of Department,	Raymond Juzaitis

May 2009

Major Subject: Nuclear Engineering

ABSTRACT

Microgravity Flow Regime Transition Modeling. (May 2009)
Adam Michael Shephard, B.S., Texas A&M University
Chair of Advisory Committee: Dr. Frederick R. Best

Flow regime transitions and the modeling thereof underlie the design of microgravity two-phase systems. Through the use of the zero-g laboratory, microgravity two-phase flows can be studied. Because microgravity two-phase flows exhibit essentially no accelerations (i.e. no buoyancy or gravitational forces), the effects of acceleration on two-phase flow can be decoupled from the effects of other fluid phenomenon. Two-phase systems on earth are understood mostly through empiricisms. Through microgravity two-phase research, a fundamental understanding of two-phase systems can be obtained and applied to both terrestrial systems in space applications.

Physically based bubbly-bubbly/slug and bubbly/slug-slug flow regime transition models are introduced in this study. The physical nature of the models demonstrates a new understanding of the governing relationships between coalescence, turbulence, void fraction, boundary layer affects, and the inlet bubble size distribution. Significantly, the new models are dimensionless in addition to being physically derived.

New and previous models are evaluated against zero-g data sets. Previous models are not accurate enough for design use. The new models proposed in this study are far more detailed than existing models and are within the precision necessary for most design purposes. Because of the limited data available, further experimental validation is necessary to formally vet the model.

Zero-g data set qualification and flight experiment design have not been standardized and as a result, much of the data in the literature can be shown not to represent

microgravity conditions. In this study, a set of zero-g quality criteria are developed and used to qualify the data sets available in the literature. The zero-g quality criteria include limitations on buoyancy forces relative to surface tension and inertial forces as well as requirements on acceleration monitoring and flow development length and time. The resulting evaluation of the data sets available in the literature unveils several experiment design shortfalls, which have resulted in data sets being misrepresented as zero-g data sets. The quality standards developed in this study should continue to be improved upon and used in the design of future zero-g fluid experiments.

The use of one-g single-phase models in approximating zero-g two-phase experimental data was successfully performed in this study. Specifically the models for pressure drop, friction factor, wall shear, and velocity profile are demonstrated.

It is recognized that the mixing apparatus will affect the flow regime transitions, specifically the distribution of bubble sizes that exit the mixing apparatus. Unfortunately, little-to-no information regarding the mixing apparatus used in past experiments can be found in the literature. This will be an area for further developmental research.

In summary, the approach to understanding and modeling two-phase phenomenon demonstrated in this study provides tools to future researchers and engineers. Special attention to data qualification and experiment standardization provides a different prospective and interpretation of the currently available data. The physically based and dimensionless modeling demonstrated in this study can be extended to other studies in the field as well as providing a basis for the application of heat transfer modeling to microgravity two-phase systems, specifically boiling and condensation.

DEDICATION

To my lifelong mentors:

Cheryl Shephard, Thomas Shephard
Barbara Shephard, John Shephard, Ina James, Leroy James
Timothy Shephard, Thomas Rogers
Luis Rodenas

ACKNOWLEDGEMENTS

I would like to thank my committee chair, Dr. Frederick R. Best, as well as my committee members, Dr. Karen Vierow and Dr. Debjyoti Banerjee.

My appreciation and congratulations go out to Dr. Cable R. Kurwitz.

Alain R. Lebrun has been a valuable mentor on many subjects, including data analysis.

My gratitude is further extended to all the faculty in the Nuclear Engineering Department in recognition of their dedication to their students, especially Dr. Pavel V. Tsvetkov.

Additional thanks is due to Marie Cronholm, John Creasy, Adam Hetzler, Kim Kaminski and Thomas Styblinski for their editorial assistance and continuous support.

NOMENCLATURE

Bo	Bond number
C	empirical constant
D	diameter
f	fluid
F	force
Fr	Froude number
g	gas
j	superficial velocity
K	empirical constant
L	length
m	mixture
n	empirical constant
p	pressure
r	radial displacement
R	radius
Re	Reynolds number
u	velocity
V	volume
y	distance from the wall
y^+	dimensionless distance from the wall
y^*	dimensionless laminar sublayer thickness
z	axial displacement
α	cross-sectional void fraction
β	volumetric void fraction
μ	viscosity
σ	surface tension
τ_w	wall shear

TABLE OF CONTENTS

CHAPTER Page

LIST OF FIGURES

FIGURE Page

LIST OF TABLES

CHAPTER I
INTRODUCTION

1.1 BACKGROUND

The future of space exploration requires scientist to re-imagine terrestrial systems for operation in non-earth environments. Two-phase flow systems are of special necessity to human space travel, however the two-phase body of knowledge is insufficient to support this effort. The complexity arises from two-phase flow being empirically and not physically understood, which limits the application of that knowledge to one-g environments. It is of great value to be able to include two-phase systems such as the Rankine cycle, heating and cooling, dehumidification, chemical refining, and recycling to the list of available space technologies. Notably, all the aforementioned technologies will be needed for long term missions which involve human travel.

Two-phase systems are being developed for use on the space station and eventually a lunar base. These systems begin with but are not limited to life support, thermal management, and power systems. The immediate interest in two-phase systems is because they are more economic than their one-phase counterparts. Two-phase flow carries more energy per unit mass than currently used one-phase systems. This translates to lower pumping power, lower mass requirements, higher efficiency, and lower costs. The development of the zero-g and lunar-g Rankine cycle to the envelope of available technologies opens the door for high power systems which would effectively remove the energy constraint from many other designs.

This thesis follows the style of the International Journal of Multiphase Flow.

On earth, zero-g two-phase research offers the potential to vastly improve the fundamental scientific understanding of one-g two-phase phenomenon. The relatively poor understanding of two-phase flow has led to reliance on empirical correlations with sizable margins of error. These empirical correlations are usually design specific and come at extremely high development costs. A fundamental understanding of two-phase flow would remove this economic barrier to system design while also making all designs, existing and future, more predictable.

This study focuses on the topic of flow regime modeling. Flow regime modeling is the study of how multiple phases will orient themselves in a system. The simple case of how a gas and a liquid would orient themselves when flowing together in a pipe is of particular interest. Flow regime maps for systems such as pipe flow are produced by experimenters and used to develop and validate two-phase flow models for use in design. The heat transfer properties of a system vary depending on the flow regime. Knowledge of the flow regime is a requirement for the development and modeling of two-phase heat transfer equipment. Also, it is valuable to the study of start-up and failure mode modeling.

The fundamental science and engineering of zero-g and one-g two-phase systems has not developed to a point of predictable system design without extensive, system-specific experimentation. This study provides several working theories, which after proper experimental validation will provide the engineering design criteria necessary for the development of microgravity two-phase systems.

1.2 FLOW REGIME MAPPING EXPERIMENTS

The experiments used to gather the flow regime data are all very similar. This section will explain how the zero-g environment of space is simulated. Further explained are the

typical experimental apparatus used to gather zero-g flow regime data and produce microgravity two-phase flow maps.

1.2.1 ZERO-G LABORATORIES AND ENVIRONMENTS

A variety of zero-g environments have been examined in an effort to determine conditions suitable for zero-g two-phase fluids research. These environments include drop towers, zero-g aircraft, NASA shuttle, International Space Station, neutral buoyancy systems, and computer simulations. The quality of the microgravity for each environment is: 10^{-3} g for zero-gravity aircraft, 10^{-4} g for a drop tower, and 10^{-5} g for the shuttle and the space station. Microgravity is a misnomer and is defined as 10^{-5} g. All successful microgravity fluid flow studies have been performed using zero-g aircraft. Zero-g aircraft create the zero-g environment by flying the trajectory shown in Figure 1.

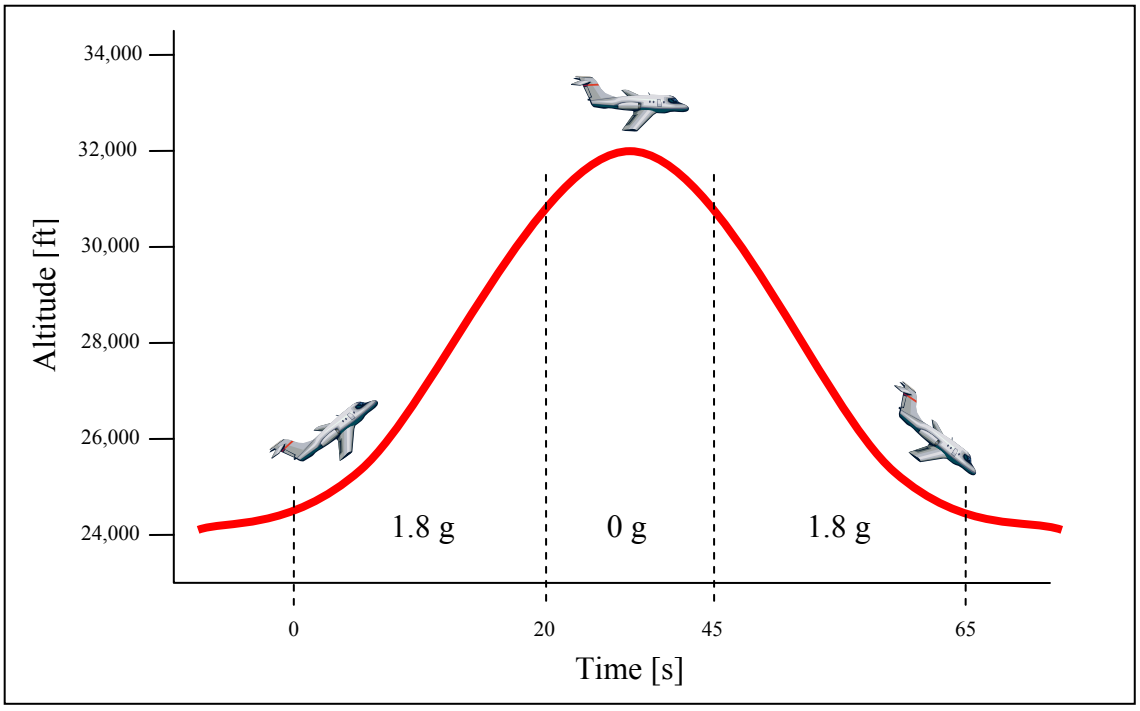

Figure 1 – Parabolic flight path of zero-g aircraft.

The limitations of zero-g aircraft are the 7-30 s window of zero-g, cost of experiments, and the 10^{-3} g limit on the quality of zero-g that can be achieved. A variety of zero-g aircraft are available with a range of 7-30 s zero-g intervals. These aircraft include:

- NASA Johnson Space Center Boeing KC-135 (retired),
- NASA Johnson Space Center McDonald Douglas C-9 (modified DC-9),
- NASA Lewis Space Flight Center Learjet 25,
- Zero-G Corp Boeing 727-200,
- French Space Agency (CNES) Caravelle, and
- Novespace Airbus A-300.

The 30 m drop tower at the NASA Lewis Space Flight Center provides 2.2 s interval of zero-g. A 105 m vacuum drop tube at the NASA Marshal Space Flight Center provides 4.6 s of zero-gravity. The Mir space station was used by Zhao, Xie, Lin, Hu, Ivanov, and Belyaev (2001) but limitations on package size and operator time did not permit adequate flow regime mapping. A neutral buoyancy experiment was attempted by Lovell (1985) where two fluids of equal density were used in one-g to simulate zero-g. The technique has not been validated. A computational experiment was conducted by Ghrist (2008) where an existing computer code, RELAP5-3D, demonstrated the limitations of currently available computational modeling when applied to zero-g conditions.

1.2.2 EXPERIMENTAL APPARATUS

All flow regime mapping experiments consist of a test section accompanied by supporting mechanical, measurement, and data acquisition equipment. A typical test section, illustrated in Figure 2, has three basic subsections: a mixing section, development section, and observation section. The mixing section is where the gas and liquid phases first come in contact. The development section allows the flow to fully develop. The observation section is where the fully developed flow regime is formally identified and recorded.

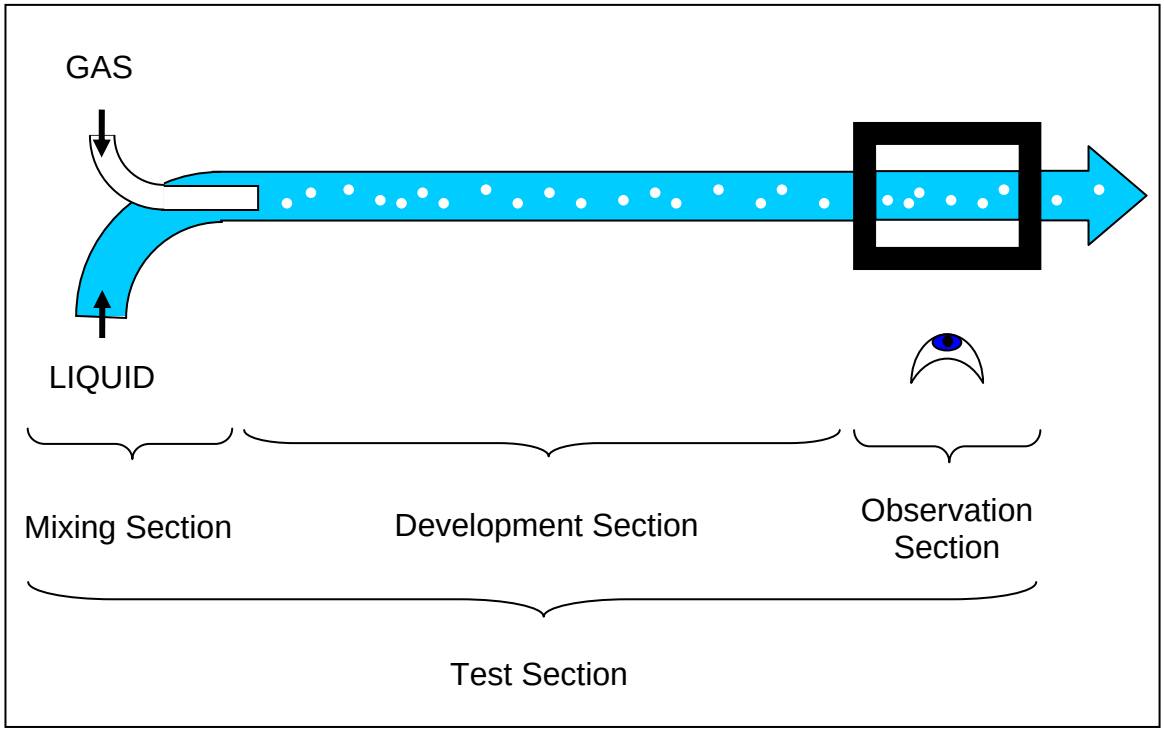

Figure 2 – Typical microgravity flow regime test section which includes a mixing section, development section, and observation section.

For the mixing section, various mixing apparatus have been used in past flow regime mapping experiments such as Venturi, perforated pipe, annular, and t-junction mixers. The mixing apparatus used in a particular experiment determines the bubble size distribution at the inlet to the development section. The development section must be sufficiently long and the pipe wall sufficiently smooth to allow the flow to fully develop. Typically, clear plastic piping is used so the flow regime development can be viewed. The observation section usually includes an optical instrument to correct for the parallax caused by the curvature of the pipe. Because fluid flows can exceed the resolution of the human eye, high speed video is used to capture the imagery for high-resolution, slow-motion playback.

Measurements of the system temperature, absolute pressure, pressure drop, and void fraction are typically taken at the appropriate points along the test section.

Measurements are typically collected using a high-speed data acquisition system. Supporting hardware includes pumps, flow rate controllers, a two-phase separator, buffer volumes, measurement equipment, and data acquisition system. Included in the measurement equipment are accelerometers which are necessary to ensure the quality of the zero-g. Typically, two independent sets of three accelerometers are attached directly to the test section to measure any mechanical vibrations the system may encounter in addition to gravitational accelerations. The three accelerometers are oriented along the three Cartesian coordinate planes to measure fore-aft, wing-to-wing, and vertical accelerations.

1.2.3 FLOW REGIME IDENTIFICATION

The arrangement of gas and liquid in a pipe is the focus of flow regime studies. The flow regime witnessed in the observation section of a flow regime experiment is dependent on system parameters, such as gas and liquid flow rates, pipe diameter, gravity, and inlet bubble size as well as fluid properties such as surface tension, densities, and viscosities. By varying these parameters, a continuous spectrum of zero-g flow regimes exists. The three general categories of flow regimes are bubbly, slug, and annular which can be further divided into the subcategories illustrated in Figure 3 with descriptions in Figure 4.

It is unclear at this time which flow regimes are caused by the imperfect zero-g aircraft environment and which are phenomenon native to zero-g. Phenomena such as wave motion, and variations in bubble sizes could easily be caused by variances in residual gravity or equipment vibration. Specifically mentioned in this study is the influence of the inlet bubble size distribution and the mixing apparatus on the observed flow regime.

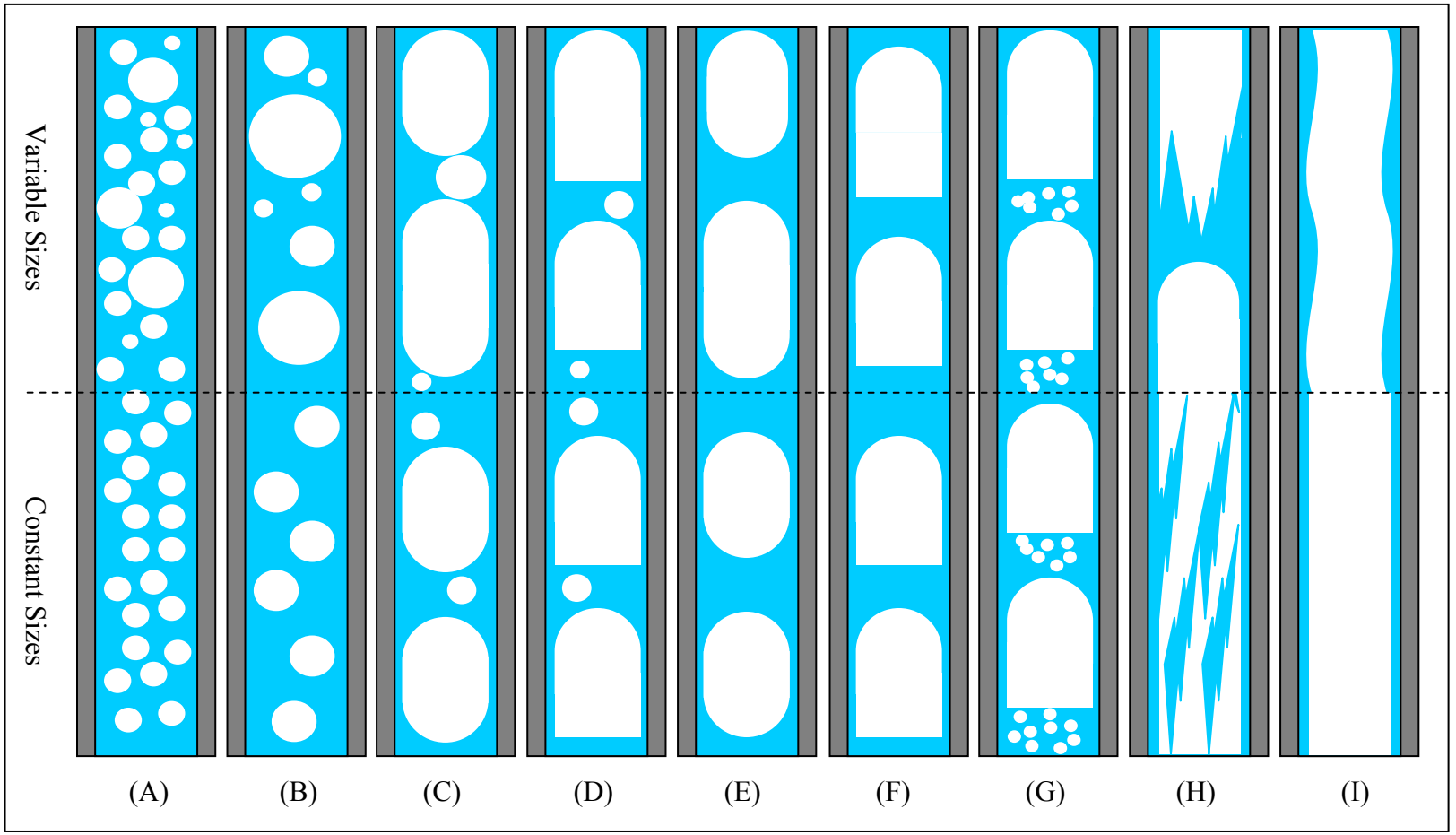

Figure 3 – Illustrations of microgravity two-phase flow regime classifications. (A) bubbly-dispersed, (B) bubbly-non-dispersed, (C) bubbly/slug-elongated and spherical, (D) bubbly/slug-Taylor and spherical, (E) bubbly/slug-elongated, (F) bubbly/slug-Taylor, (G) slug-Taylor with dispersed, (H) slug/annular, and (I) annular. Descriptions of the flow regimes are presented in Figure 4.

(A) Bubbly – Dispersed

More than two bubbles can be found in a representative cross-section of the pipe. Bubbles sizes can be uniform or distributed.

(B) Bubbly – Non-Dispersed

One or two bubbles can be found in a representative cross-section of the pipe. Bubbles sizes can be uniform or distributed.

(C) Bubbly/Slug – Elongated and Spherical

Both spherical and elongated bubbles are present. Bubbles sizes can be uniform or distributed.

(D) Bubbly/Slug – Taylor and Spherical

Both spherical and Taylor bubbles are present. Bubbles sizes can be uniform or distributed.

(E) Slug – Elongated

Elongated bubbles are present. Bubbles sizes can be uniform or distributed.

(F) Slug – Taylor

Taylor bubbles are present. Bubbles sizes can be uniform or distributed.

(G) Slug – Taylor and Dispersed

Taylor bubble with trailing dispersed spherical bubbles. Bubbles sizes be can uniform or distributed.

(H) Slug/Annular

Chaotic flow. Dispersed bubbles may or may not be observed. Annular and slug regimes may intermittently be observed. "Bridges" may be observed, which cause a transition from annular-to-slug. Coalescence of two elongated bubbles may be observed which cause a transition from slug-to-annular.

(I) Annular

Gas core with a liquid annulus. The gas-liquid interface can be described as either smooth or wavy. Kinematic waves may be observed.

Figure 4 – Descriptions of microgravity two-phase flow regime classifications shown in Figure 3.

CHAPTER II
DATA PRESENTATION

2.1 INTRODUCTION

All data sets presented in this chapter were produced using the general experimental apparatus explained in Chapter I with mention of each experiment's unique attributes. These unique attributes are the zero-g aircraft type, acceleration monitoring apparatus, residual acceleration cut-offs, development lengths and times, temperatures, pressures, test section orientation within the aircraft, and mixing apparatus type. Also, some data sets recognize the bubbly/slug flow regime while other do not.

2.2 HEPPNER ET AL. 1975

The results of the Heppner, King, and Littles (1975) experiment demonstrated that flow regimes are different in zero-g than in one-g. This 0.0254 m diameter air-water system was operated onboard the NASA Johnson Space Center KC-135 aircraft. The development length of 20 length/diameters (L/D) was observed by the experimenters to be insufficient for flow to fully develop. The zero-g window was 15-20 s. Mono-axial acceleration monitoring was used. The test section pressure and temperature was not reported. The orientation and location of the test section with respect to the aircraft are unknown. The mixing apparatus used in the experiment is unknown.

2.3 DUKLER ET AL. 1988/JANICOT 1988

The Dukler, Fabre, McQuillen, and Vernon (1988) study was the first detailed flow regime mapping experiment which produced high quality results. A separate account of this experiment appeared in Janicot (1988) which included additional data points. Two different experiments were conducted in the course of the study. The first of the two

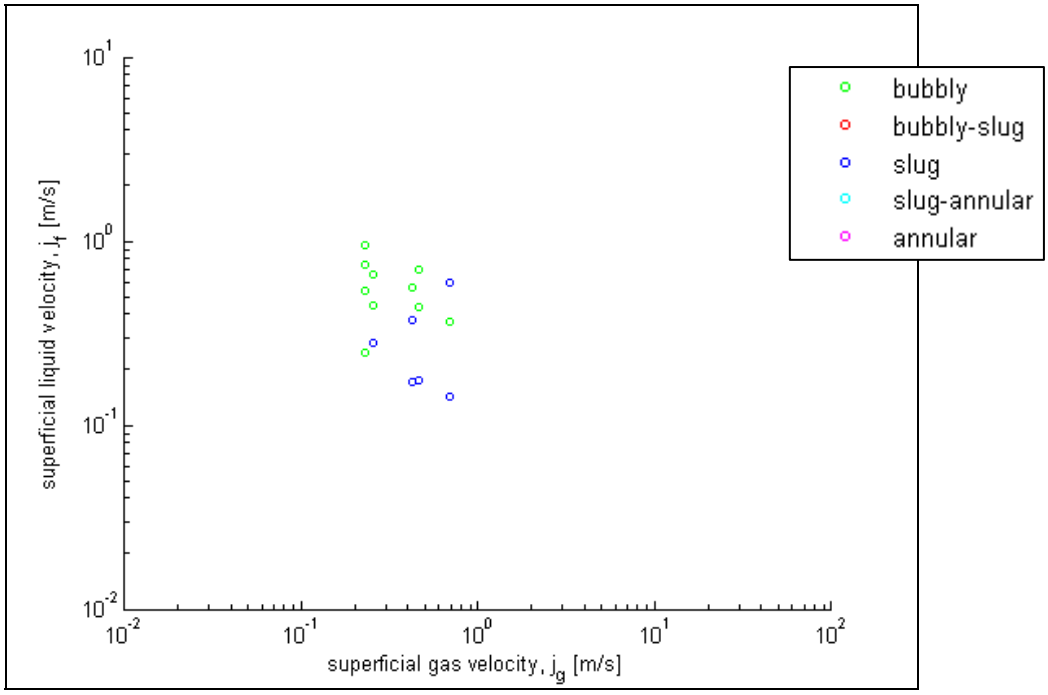

Figure 5 – Dukler et al. (1988) 0.009525 m diameter air-water data set.

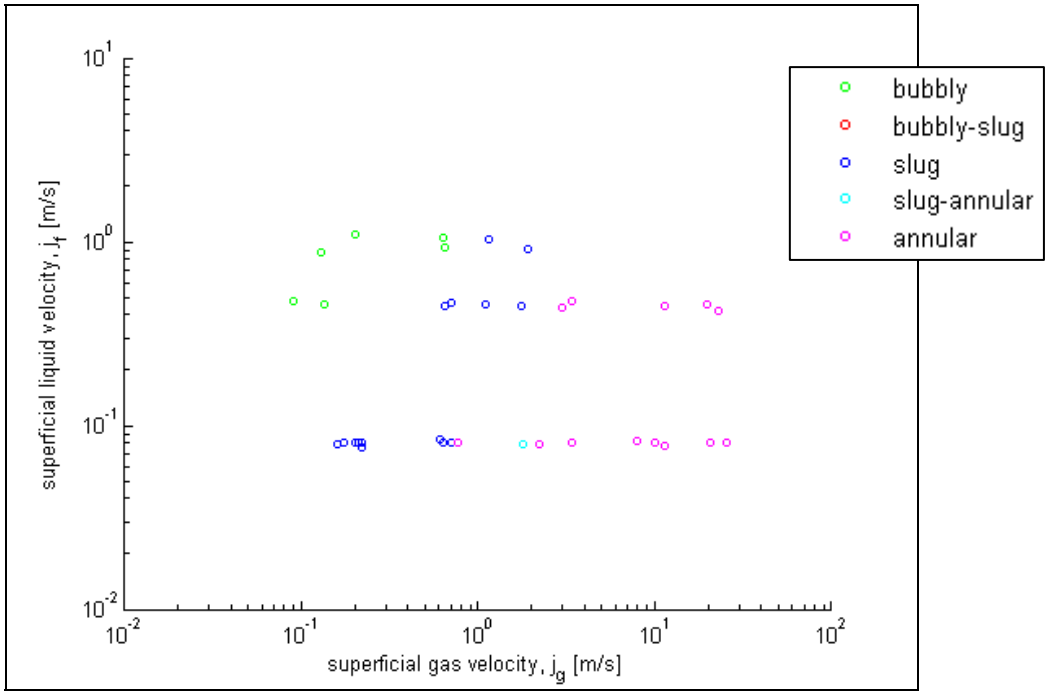

Figure 6 – Dukler et al. (1988) 0.0127 m diameter air-water data set.

experiments was conducted in a drop tower, the second experiment was conducted in a zero-gravity aircraft.

The first of the Dukler et al. (1988) experiments was a 0.009525 m diameter air-water system operated during free fall using the NASA Lewis 30 m Drop Tower. The 2.2 s drop interval was observed by experimenters to be insufficient time for the flow to fully develop. The development length of the system was 48 L/D. The test section pressure and temperature was not reported. The orientation and location of the test section with respect to vertical is unknown. The mixing apparatus used in the experiment was a perforated pipe. The collected data are shown in Figure 5.

The second experiment was a 0.0127 m diameter air-water system operated onboard the NASA Lewis Learjet. The development length of 83 L/D and the 12-22 s window of zero-g were observed by the experimenters to be sufficiently long for flow to fully develop. The tri-axial acceleration cut-off was chosen to be 0.02 g. The pressure and temperature of the fluids were not reported. The orientation of the test section relative to the aircraft is unknown. The mixing apparatus used on the experiment is unknown. This data set does not recognize the bubbly/slug regime in its characterization of flow regimes. The collected data are shown in Figure 6.

2.4 COLIN ET AL. 1991

The Colin, Fabre, and Dukler (1991) experiment was the first zero-g flow regime mapping study to use a large diameter pipe, include void fraction measurements, take bubble diameter measurements at the entrance and exit of the test section, and extend well above a Reynolds number of 10,000. A separate account of this experiment appeared in Colin (1990). The bubble diameter measurements demonstrated the extent to which bubbles coalesce along a test section and suggest the role of coalescence in flow regime development. Large buoyancy forces are characteristic of the large pipes and the experimenters stated that the buoyancy forces may have influenced the observed

flow regimes. This 0.0400 m diameter air-water system was operated on the French Space Agency (CNES) Caravelle aircraft. The development length of 80 L/D and the zero-g window of 15-20 s were observed by the experimenters to be sufficiently long for flow to fully develop. The mono-axial acceleration cut-off was chosen to be 0.03 with an additional exclusion of data points which had a Froude number value of less than 5. The test section pressure of 80 kPa was reported, however, the temperature was not. The orientation and location of the test section with respect to the aircraft are unknown. The mixing apparatus used in the experiment was a Venturi mixer. This data set does not recognize the bubbly/slug regime in its characterization of flow regimes. The collected data are shown in Figure 7.

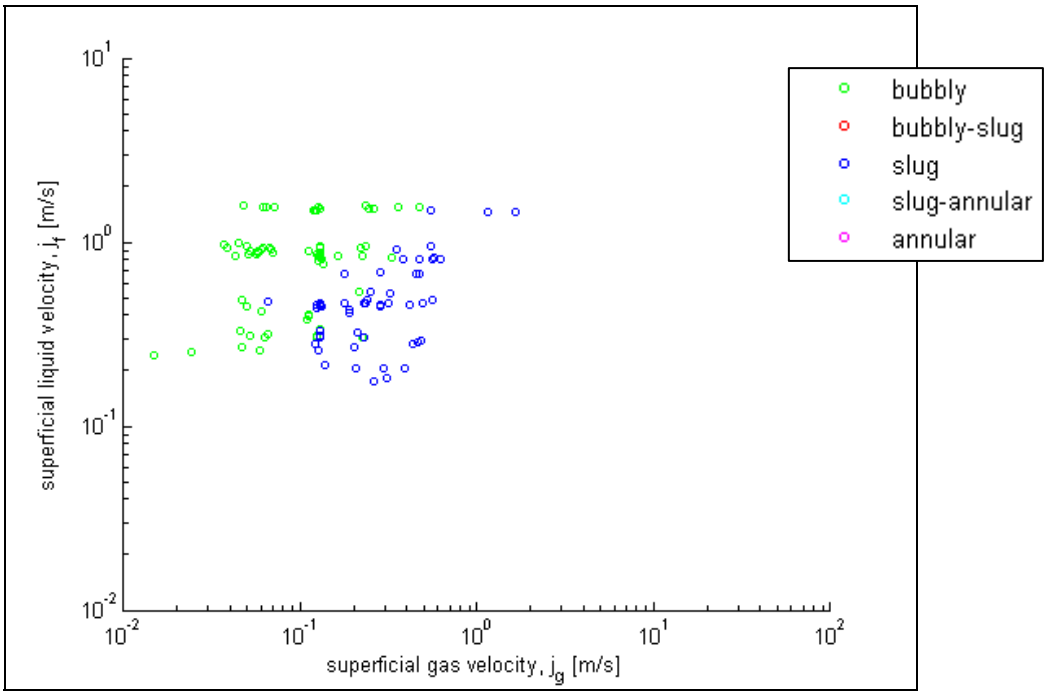

Figure 7 – Colin et al. (1991) 0.0400 m diameter air-water data set.

2.5 HUCKERBY AND REZKALLAH 1992

The Huckerby and Rezkallah (1992) experiment was a 0.009525 m diameter air-water system operated onboard the NASA JSC KC-135 aircraft. The development length of 90 L/D and the zero-g window of 20 s were observed by the experimenters to be sufficiently long for flow to fully develop. The mono-axial acceleration cut-off was chosen to be 0.05 g. The test section pressure and temperature was not reported. The orientation of the test section with respect to the aircraft is unknown, and its location was in the rear of the aircraft. The mixing apparatus used in the experiment was an injector nozzle. The collected data are shown in Figure 8.

2.6 ZHAO AND REZKALLAH 1993

The Zhao and Rezkallah (1993) experiment was a 0.009525 m diameter air-water system and was operated on the NASA Johnson Space Center KC-135 aircraft. The development length of 80 L/D and the zero-g window of 20 s were observed by the experimenters to be sufficiently long for flow to fully develop. The mono-axial acceleration cut-off was chosen to be 0.03 g. The experimenters state that buoyancy forces may have affected the observed flow regimes. The test section pressure of 55-83 kPa and temperature of 25-40 ^{o}C were reported. The orientation of the test section with respect to the aircraft was vertical and its location is unknown. The mixing apparatus used in the experiment was a perforated pipe mixer. This data set does not recognize the bubbly/slug regime in its characterization of flow regimes. The collected data are shown in Figure 9.

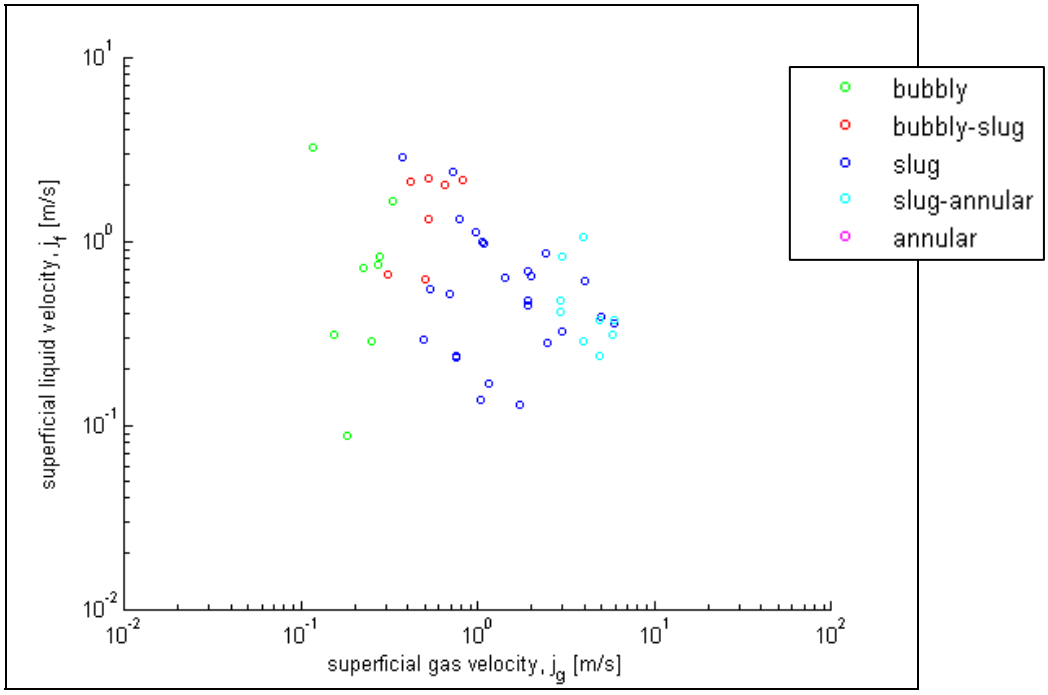

Figure 8 – Huckerby and Rezkallah (1992) 0.009525 m diameter air-water data set.

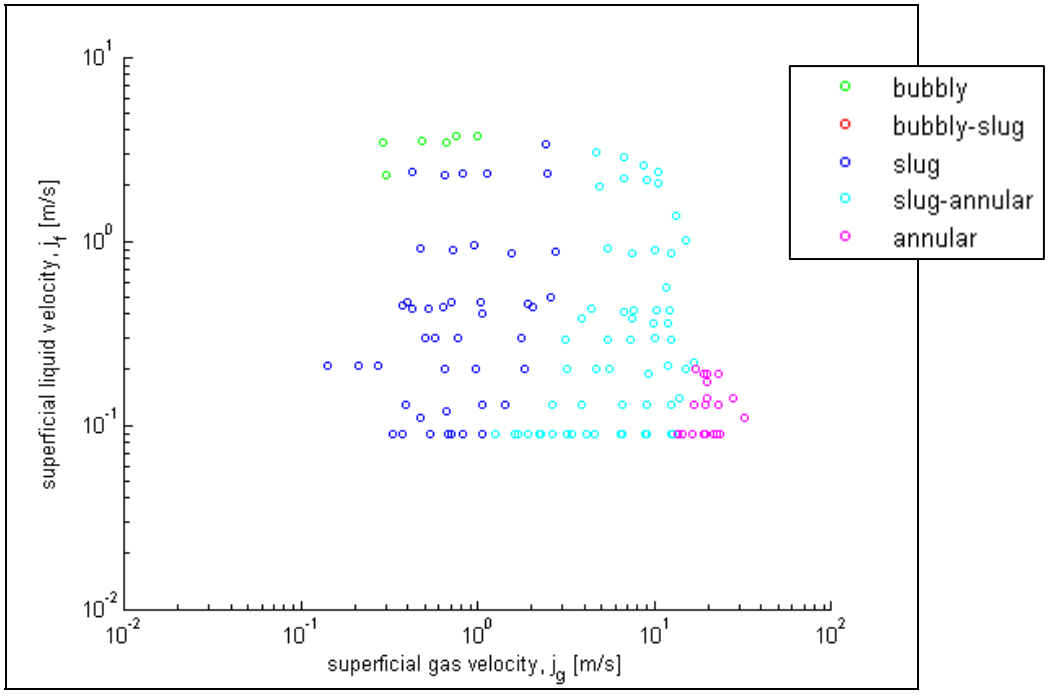

Figure 9 – Zhao and Rezkallah (1993) 0.009525 m diameter air-water data set.

2.7 BOUSMAN 1994

The Bousman (1994) study was the first to systematically investigate the influence of pipe diameter, surface tension, and viscosity on flow regime transitions. The fluids used in the study were air-water, air-water/50-50%wt glycerin, and air-water/0.5%wt Zonyl FSP. Both glycerin and Zonyl FSP have approximately the same properties as water except that glycerin has a much higher viscosity and Zonyl has a much lower surface tension. Six separate data sets were generated during two separate flight campaigns.

For the first campaign, 0.0127 m diameter air-water, air-water/glycerin, and air-water/Zonyl FSP systems, were operated onboard the NASA Lewis Learjet 25. The development length of 84 L/D and the zero-g window of 7-15 s were observed by the experimenters to be sufficiently long for flow to fully develop. Void fraction and annular film thickness measurements were collected. The collected air-water data are shown in Figure 10.

For the second campaign, 0.0254 m diameter air-water, air-water/glycerin, and air-water/Zonyl FSP systems were operated onboard the NASA Johnson Space Center KC-135. The development length of 79 L/D and the zero-g window of 7-15 s were observed by the experimenters to be sufficiently long for flow to fully develop. The results are shown in Figure 11.

For both flight campaigns, the tri-axial acceleration cut-off was chosen to be 0.02 g. The test section temperature ranged from 19-23 ^{o}C while the pressure was not reported. The orientation and location of the test sections with respect to the aircraft were not reported. The mixing apparatus used in these experiments were an annular mixer.

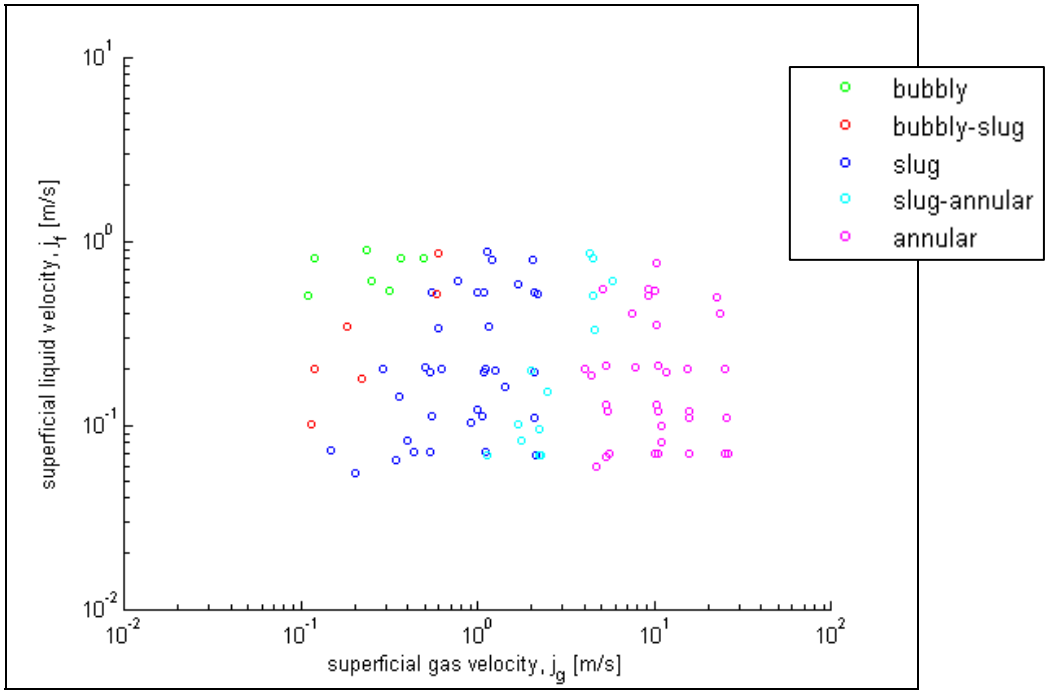

Figure 10 – Bousman (1994) 0.0127 m diameter air-water data set.

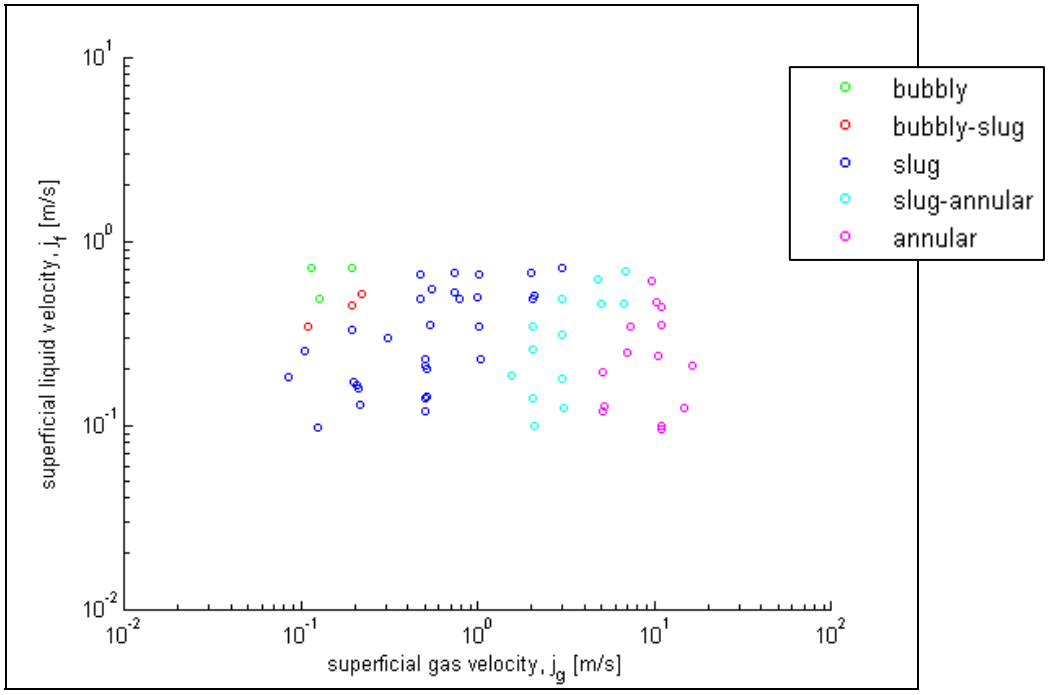

Figure 11 – Bousman (1994) 0.0254 m diameter air-water data set.

2.8 COLIN AND FABRE 1995

The Colin and Fabre (1995) experiment provides the highest quality data sets found in the literature and includes void fraction and pressure drop measurements. This study of 0.0060, 0.0100, and 0.0190 m air-water systems was operated onboard the French Space Program (CNES) Caravelle. The development length of 80 L/D and the zero-g window of 7-15 s were observed by the experimenters to be sufficiently long for flow to fully develop. The tri-axial acceleration cut-off was chosen to be 0.02 g. The test section pressure and temperature was not reported. The orientation of the test section with respect to the aircraft floor was horizontal while the location is unknown. The mixing apparatus used in the experiment was a Venturi mixer. The collected data are shown in Figure 12 through Figure 14.

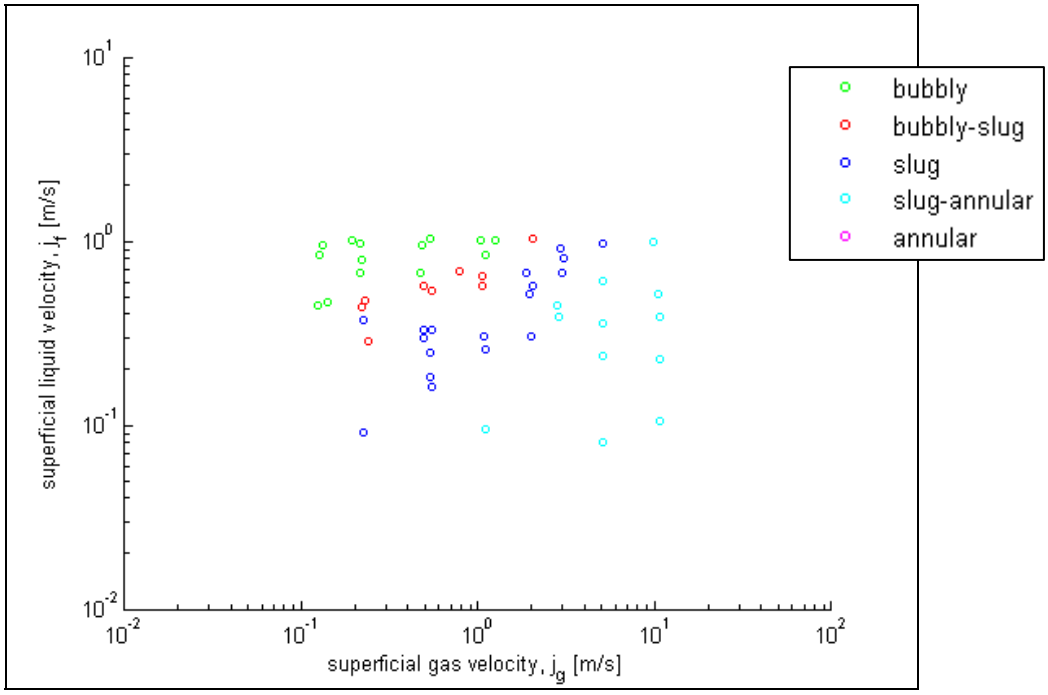

Figure 12 – Colin and Fabre (1995) 0.0060 m diameter air-water data set.

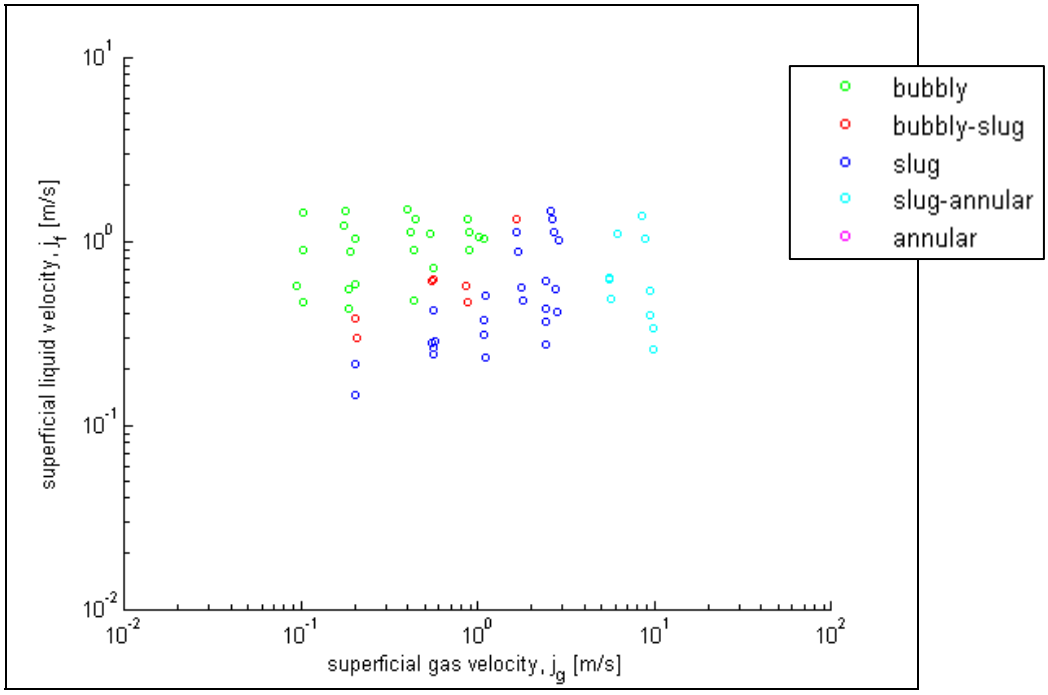

Figure 13 – Colin and Fabre (1995) 0.0100 m diameter air-water data set.

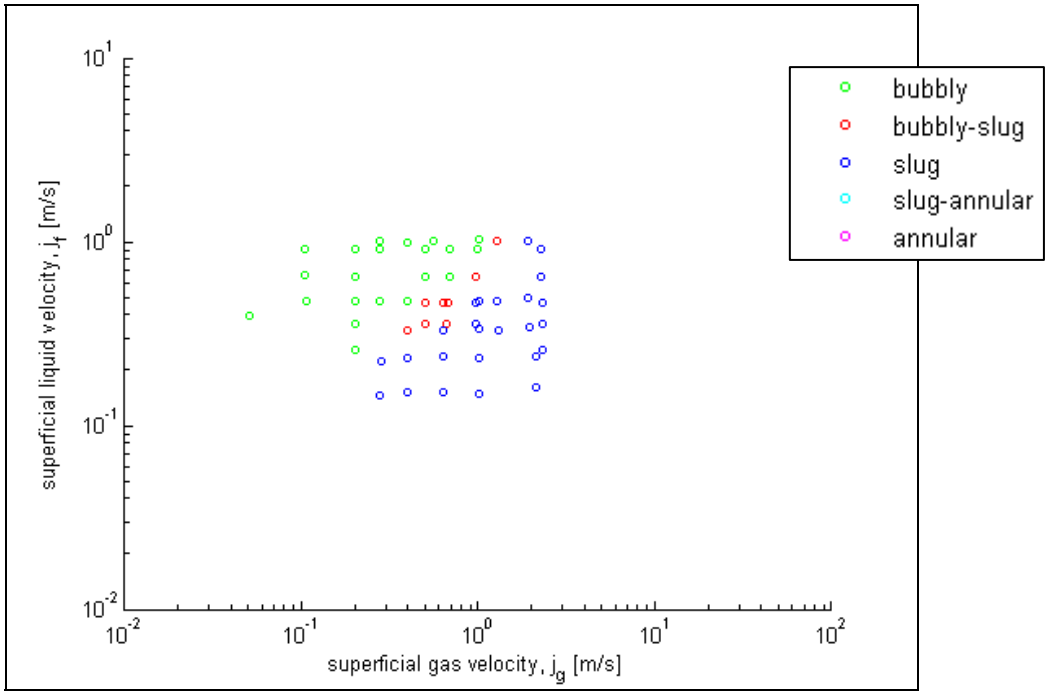

Figure 14 – Colin and Fabre (1995) 0.0190 m diameter air-water data set.

2.9 SUMMARY

The data sets currently available in the literature for zero-g air-water systems were presented in this chapter. The techniques used in collecting the various zero-g data sets are all generally similar and the known differences in the experiments are summarized in Table 1.

Table 1 – Summary of zero-g air-water data sets.

Researcher	Pipe Dia. [m]	Accel. Monitor Type	Accel. Cutoff [g]	Facility	Mixing Apparatus	Devel. Length [L/D]	Devel. Time [s]
Heppner et al. 1975	0.0254	none	n/a	KC-135	T-junction	20	15-20
Dukler et al. 1988	0.0095	none	n/a	drop tower	perf. pipe	48	2.2
	0.0127	tri-ax.	0.02	Learjet	unknown	83	12-22
Colin et al. 1991	0.0400	mono-ax.	0.03	Caravelle	Venturi	79	15-20
Huckerby and Rezkallah 1992	0.0095	mono-ax.	0.05	KC-135	nozzle	90	20
Zhao and Rezkallah 1993	0.0095	mono-ax.	0.03	KC-135	perf. pipe	80	20
Bousman 1994	0.0127	tri-ax.	0.02	Learjet	annular	87	7-15
	0.0254	tri-ax.	0.02	KC-135	annular	79	7-15
Colin and Fabre 1995	0.0060	tri-ax.	0.02	Caravelle	Venturi	80	7-15
	0.0100	tri-ax.	0.02	Caravelle	Venturi	80	7-15
	0.0190	tri-ax.	0.02	Caravelle	Venturi	80	7-15

CHAPTER III
DATA QUALIFICATION

3.1 INTRODUCTION

With regard to the data sets presented in Chapter II, several of the experimenters mentioned that buoyancy effects were observed during their data collection and may have influenced the observed flow regimes. This chapter develops zero-g quality criteria to determine if a data set is truly representative of microgravity flows or is overly influenced by residual accelerations. Development length and time criteria are also developed. Also included in this chapter is a discussion of other sources of data collection errors leading to the misinterpretation of data sets.

3.2 RESIDUAL ACCELERATIONS

Buoyancy forces are a function of acceleration, the difference in fluid densities, and bubble size. Acceleration monitoring during zero-g experiments provides information related to the magnitude of inevitable buoyancy forces. Because buoyancy forces are not present in true microgravity, it is essential that they do no influence experiment results. Suitable acceleration monitoring and limitations on buoyancy forces relative to other forces are thus necessary when qualifying a data set as zero-g.

3.2.1 MONO-AXIAL VS. TRI-AXIAL ACCELERATION MONITORING

Experimentalists have monitored accelerations using either mono-axial or tri-axial accelerometers. The accuracy of a data set can be gauged by the quality of the zero-g environment from which the data were collected. Mono-axial acceleration monitoring does not account for lateral and fore-aft accelerations. Because the lateral and fore-aft accelerations are known to be significant (Reinarts 1993, Bousman 1994), data sets

produced with mono-axial acceleration monitoring cannot be assumed accurate. Tri-axial acceleration monitoring is necessary to certify the zero-g quality of a data set.

3.2.2 ACCELERATION CUT-OFF

It is unknown at this time how much residual gravity is an acceptably approximation of zero-g. It is suggested by Colin et al. (1991) that the 10^{-3} g environment of the zero-g aircraft may be insufficient for zero-g flow regime mapping of large diameter pipes (in reference to a 0.0400 m air-water system).

Clearly when buoyancy forces near the magnitude of surface tension and inertial forces, the data cannot be assumed to approximate zero-gravity. To determine the minimal acceptable residual gravity, the buoyancy force of a bubble with a diameter of the pipe is compared to the accompanied surface tension and inertia forces.

3.2.2.1 BOND NUMBER LIMIT

The Bond number (*Bo*) is the dimensionless number representing the buoyancy force over the surface tension force and is shown in (3.1).

$$Bo = \frac{buoyancy\ force}{surface\,tension\ force} = \frac{\left(\rho_f - \rho_g\right) D^2 g}{\sigma} \tag{3.1}$$

In equation (3.1), *Bo* is the Bond number, ρ_i is the density for phase *i*, *D* is the pipe diameter, *g* is acceleration, σ is surface tension, and the *f* and *g* subscripts distinguish the liquid and gas properties, respectively. Separately, a force balance of the buoyancy forces and the surface tension forces acting on a bubble with a diameter equal to that of the pipe is performed in (3.2) through (3.5).

$$\frac{F_B}{F_\sigma} = 1 \tag{3.2}$$

$$F_\sigma = \sigma \pi D \tag{3.3}$$

$$F_B = \left(\rho_f - \rho_g\right) V g = \left(\rho_f - \rho_g\right) \frac{\pi}{6} D^3 g \tag{3.4}$$

$$\frac{\left(\rho_f - \rho_g\right) \frac{\pi}{6} D^3 g}{\sigma \pi D} = \frac{\left(\rho_f - \rho_g\right) \frac{1}{6} D^2 g}{\sigma} = 1 \tag{3.5}$$

In equations (3.2) through (3.5), F_B is the buoyancy force, F_σ is the surface tension force, and V is bubble volume. The Bond number from (3.1) is then substituted into (3.5) and solved.

$$\frac{1}{6} Bo = \frac{F_B}{F_\sigma} = \frac{\left(\rho_f - \rho_g\right) \frac{1}{6} D^2 g}{\sigma} = 1 \tag{3.6}$$

$$Bo = 6 \frac{F_B}{F_\sigma} = \frac{\left(\rho_f - \rho_g\right) \frac{1}{6} D^2 g}{\sigma} = 6 \tag{3.7}$$

A $Bo = 6$ means the buoyancy and surface tension forces are equivalent. For the purposes of quality control of an experiment, the buoyancy forces are suggested to be an order of magnitude less than the surface tension forces. This stipulation sets the maximum allowable Bond Number to 0.6. The Bond Number is recognized to be constant for all data points across a data set.

$$\max\left(Bo\right) = 0.60 \tag{3.8}$$

3.2.2.2 FROUDE NUMBER LIMIT

The Froude Number (*Fr*) is the dimensionless number representing the inertial force over the buoyancy force and is shown in (3.9).

$$Fr = \frac{inertial\ force}{buoyancy\ force} = \sqrt{\frac{\rho_f j_f^2 + \rho_g j_g^2}{\left(\rho_f - \rho_g\right) Dg}} \tag{3.9}$$

In equation (3.9), *Fr* is the Froude number, ρ_i is the density for phase i, j_i is the superficial velocity for phase i, D is the pipe diameter, g is acceleration, and the f and g subscripts distinguish the liquid and gas properties, respectively. Separately, a force balance of the inertial forces and the buoyancy forces acting on a bubble with a diameter equal to that of the pipe is performed in (3.10) through (3.13).

$$\frac{F_I}{F_B} = 1 \tag{3.10}$$

$$F_I = \rho_m u_m^2 A_C = \left(\rho_f j_f^2 + \rho_g j_g^2\right)\frac{\pi}{4} D^2 \tag{3.11}$$

$$F_B = \left(\rho_f - \rho_g\right) gV = \frac{\pi}{6}\left(\rho_f - \rho_g\right) gD^3 \tag{3.12}$$

$$\frac{F_I}{F_B} = \frac{\frac{\pi}{4}\left(\rho_f j_f^2 + \rho_g j_g^2\right) D^2}{\frac{\pi}{6}\left(\rho_f - \rho_g\right) gD^3} = \frac{\left(\rho_f j_f^2 + \rho_g j_g^2\right)}{\frac{2}{3}\left(\rho_f - \rho_g\right) gD} = 1 \tag{3.13}$$

In (3.10) through (3.13). F_I is the inertial force, F_B is the buoyancy force, u_m is the mixture velocity, A_C is the cross-sectional area of the pipe, and V is bubble volume. The Froude number from (3.9) is then substituted into (3.13) and then solved.

$$\frac{3}{2}Fr^2 = \frac{F_I}{F_B} = \frac{\left(\rho_f j_f^2 + \rho_g j_g^2\right)}{\frac{2}{3}\left(\rho_f - \rho_g\right)gD} \tag{3.14}$$

$$Fr = \sqrt{\frac{2}{3}\frac{F_I}{F_B}} = \sqrt{\frac{\frac{2}{3}\left(\rho_f j_f^2 + \rho_g j_g^2\right)}{\frac{2}{3}\left(\rho_f - \rho_g\right)gD}} = \sqrt{\frac{2}{3}} = 0.8165 \tag{3.15}$$

A $Fr = 0.82$ means the inertial and buoyancy forces are equivalent. For the purposes of quality control of an experiment, the inertial forces are suggested to be an order of magnitude greater than the buoyancy forces. This stipulation sets the minimum allowable Froude number to 2.6. The Froude number is associated with individual data points and varies across a data set.

$$\min\left(Fr\right) = 2.6 \tag{3.16}$$

It is further noted that Colin et al. (1991) observed that for a 0.0400 m diameter air-water system that $Fr < 5$ produced unacceptable levels of gravity, causing flows to become asymmetric. $Fr = 5$ is equivalent to an inertial-to-buoyancy force ratio of 38:1.

$$Fr = \sqrt{\frac{2}{3}\frac{F_I}{F_B}} = 5 \quad \Leftrightarrow \quad \frac{F_I}{F_B} = 38 \tag{3.17}$$

3.3 FLOW DEVELOPMENT

In order to compare the flow regime observations across different data sets, conditions must be similar. The most suitable comparison is made when flow regimes are fully developed. The appropriate conditions to ensure that flow is fully developed are developed in this section.

3.3.1 DEVELOPMENT LENGTH

To determine the development length necessary for flow to fully develop, the representative cases of 0.009525 m (small), 0.0127 m (medium), and 0.0254 m (large) diameter systems are discussed. Huckerby (1992) reported that 30 L/D was a sufficient development length for a zero-g 0.009525 m pipe diameter air-water system. Bousman (1994) reported that 24 L/D was a sufficient development length for 0.0127 and 0.0254 m pipe diameter systems for use with air-water, air-water/glycerin, and air-water/Zonyl FSP.

The aforementioned reports are consistent with that of one-g. From the experimenters claims, it is assumed that the flow development length necessary for zero-g can be conservatively approximated by that of one-g. Thus for zero-g the following development lengths are assumed to be a minimum requirement.

$$\min(\textit{development length}\ [L/D]) = 0.05Re \qquad Re < 2100 \qquad (3.18)$$

$$\min(\textit{development length}\ [L/D]) = 40 \qquad Re > 2100 \qquad (3.19)$$

In equations (3.18) and (3.19), *Re* is the Reynolds number.

3.3.2 DEVELOPMENT TIME

Dukler et al. (1988) and Zhao and Rezkallah (1993) analyzed the films from their experiments and concluded that flow patterns and other characteristics became constant 1 to 3 s after transitioning to zero-g. Dukler et al. (1988) also calculated that a continuity wave took a maximum of 1.2 s to traverse his test section which was 1.06 m long (or 83 L/D). It is noted that any disturbances in flow development require time for the entire test section to clear. The time it takes to clear the test section is in addition to the 3 s it

takes for the flow to stabilize after the gravity transition. Thus for zero-g the following development time is assumed to be a minimum requirement.

$$\min(\textit{development time}\ [s]) = 3 + uL \tag{3.20}$$

In equation (3.20), u is the velocity and L is the test section length.

3.4 ADDITIONAL SOURCES OF ERRORS

Other uncertainties exist in the data which are too obscure to quantify. Nonetheless, researchers should be alerted to their presence and significance when interpreting the data presented in Chapter II.

3.4.1 FLOW REGIME SUBJECTIVITY

There is not a universally accepted set of flow regimes. Flow regimes mentioned in the literature vary from source to source. Many common flow regimes have been differentiated into subcategories which were presented in Figure 3 and Figure 4.

3.4.2 MIXING APPARATUS AND PIPE ROUGHNESS

The mixing apparatus and pipe roughness vary from experiment to experiment and are so far not quantified in the literature. The mixing apparatus controls the inlet bubble size distribution, and the pipe roughness controls pressure drop and wall friction effects. These two differences can be expected to affect the flow regime, thus, the best comparisons are made between data sets produced on the same/similar test sections.

3.4.3 EXPERIMENT PLACEMENT AND ORIENTATION ON THE AIRCRAFT

Angular acceleration along the wing-to-wing axis of rotation occurs while the microgravity aircraft traverses the zero-g parabola. The further the experiment is placed from the wing-to-wing axis of rotation, the greater the acceleration felt by the experiment.

Transverse and fore-aft accelerations are significantly large (Reinarts 1993, Bousman 1994) and can not be assumed negligible. Linear acceleration fluctuations are largest along the gravitational vector and smallest along the transverse vector between the wings. Horizontally oriented systems also benefit from observable indicators of acceleration effects such as asymmetrical flow.

In summary, *the ideal placement of an experiment onboard a zero-g aircraft is directly between the wings with the direction of flow being horizontal from wing to wing*. All other choices for experiment placement and orientation reduce data quality.

3.4.4 PRESSURE AND TEMPERATURE

Many experiments neglect to report system pressures and temperatures with the data. Without these measurements, fluid properties must be assumed to be those at room temperature and atmospheric pressure. It is known that temperatures onboard zero-g aircraft are flight dependent and change over the course of the flight. To bring attention to the errors incurred by assuming a constant system pressure and temperature, Table 2 lists the fluid property variations for the system temperatures and pressures reported by Zhao (1993) for a 0.009525 m diameter air-water system. The system temperature and pressure varied from 35-40 ^{o}C and 55-83 kPa during the flight campaign. It is shown in Table 2 that air density varies significantly for small changes in temperature and

pressure while the other fluid properties do not. For high gas flow rates, where the gas phase carries a significant proportion of the flow momentum, this error becomes large.

Table 2 – Fluid property variation for air and water with temperature and pressure ranging from 35-40 ^{o}C and 55-83 kPa.

	Water	Air
Density [kg/m^3]	993.1 +/- 0.09%	0.7752 +/- 21%
Surface tension [N/m]	0.0700 +/- 0.6%	n/a
Viscosity [kg/m-s]	0.0006865 +/- 0.05%	0.00001907 +/- 0.6%

3.5 SUMMARY

The quality criteria for a data set to be considered representative of zero-g was determined in this chapter. The quality criteria are summarized in Table 3 and include tri-axial acceleration monitoring, limits on buoyancy forces relative to surface tension and inertial forces, and requirements for development length and time. Additional sources of experimental error include the subjectivity of flow regime observations, variations in mixing apparatus and pipe roughness, assumptions about system temperatures and pressures, and test section orientation and location relative to the aircraft floor and axis of rotation.

Table 3 – Summary of zero-g qualification criteria.

acceleration monitoring type	tri-axial	
Froude number (*Fr*)	> 2.6	
Bond number (*Bo*)	< 0.60	
development length [L/D]*	> 40	(*turbulent*)
	> 0.05 *Re*	(*laminar*)
development time [s]*	> 3 + *uL*	

**Re* is the Reynolds number, *D* is the pipe diameter, *u* is the velocity and *L* is the test section length.

CHAPTER IV
DATA EVALUATION

4.1 INTRODUCTION

In this chapter, each data set presented in Chapter II is evaluated using the zero-g quality criteria developed in Chapter III. The data sets that meet the quality criteria will be assumed accurate and used to gage current models later in this study.

4.2 DATA EVALUATION

The criteria used for data qualification set forth in Chapter III are shown in Table 3. The characteristic values pertaining to zero-g qualification for each data set are tabulated and evaluated in Table 4.

Table 4 – Data set evaluation summary.

Researcher	Pipe Dia. [m]	Accel. Monitor Type	Accel. Cutoff [g]	Fr*	Bo	Devel. Length [L/D]	Devel. Time [s]	Zero-g Qualified?
				Fr>2.6	**Bo<0.60**	**x>40**	**t>3**	
Heppner et al. 1975	0.0254	none	n/a	n/a	n/a	20	7-22	N
Dukler et al. 1988	0.009525	none	n/a	n/a	n/a	48	2.2	N
	0.0127	tri	0.02	1.5-22	0.44	83	7-22	Y
Colin et al. 1991	0.0400	mono	0.03	1.6-14	6.5	79	7-22	N
Huckerby and Rezkallah 1992	0.009525	mono	0.05	1.3-47	0.62	90	7-22	N
Zhao and Rezkallah 1993	0.009525	mono	0.03	1.7-70	0.38	80	7-22	N
Bousman 1994	0.0127	tri	0.02	1.1-19	0.43	87	7-22	Y
	0.0254	tri	0.02	1.4-10	1.7	79	7-22	N
Colin and Fabre 1995	0.0060	tri	0.02	2.7-30	0.10	80	7-22	Y
	0.0100	tri	0.02	3.3-33	0.27	80	7-22	Y
	0.0190	tri	0.02	2.4-17	0.98	80	7-22	N

* Fr values are a function of the flow velocities and are calculated for each individual data point. Data points with an adequate Fr value will be distinguished from inadequate data points in the subsequent analysis.

4.3 ANALYSIS

A few observations can be made when comparing the qualified data sets to the non-qualified data sets. First, a comparison is made between the qualification status of a data set and the critical void fraction values corresponding to the bubbly-slug transition. Second, a comparison is made between the qualification status and reproducibility.

4.3.1 CRITICAL VOID FRACTION

Along with each data set, many experimenters have reported a critical void fraction value corresponding to the bubbly-to-slug transition. Colin et al. (1996) tabulated these reported critical void fraction values which are reproduced in Table 5. For the data sets that did not report a critical void fraction, Colin et al. (1996) estimated the value using the equation $\alpha_{cr} = C_0\beta_{cr}$ where $\beta_{cr} = j_g / (j_g + j_f)$ and $C_0 = 1.21$. For ready comparison, the buoyancy qualification information from Table 4 also appears in Table 5.

Table 5 – Correlation between zero-g qualified data sets and the critical void fraction values tabulated by Colin et al. (1996).

Researcher	Pipe Dia. [m]	Accel. Monitor Type	Bo	Zero-g Qualified?	*Critical Void Fraction
Heppner et al. 1975	0.0254	none	n/a	N	n/a
Dukler et al. 1988	0.009525	none	n/a	N	n/a
	0.0127	tri-ax	0.44	Y	0.45*
Colin et al. 1991	0.0400	mono-ax	6.5	N	0.20
Huckerby and Rezkallah 1992	0.009525	mono-ax	0.62	N	0.25*
Zhao and Rezkallah 1993	0.009525	mono-ax	0.38	N	0.18*
Bousman 1994	0.0127	tri-ax	0.43	Y	0.40
	0.0254	tri-ax	1.7	N	0.23*
Colin and Fabre 1995	0.0060	tri-ax	0.10	Y	0.45
	0.0100	tri-ax	0.27	Y	0.45
	0.0190	tri-ax	0.98	N	0.45

* critical void fraction values were not measured directly but calculated using $\alpha_{cr} = C_0\beta_{cr}$ where $\beta_{cr} = j_g / (j_g + j_f)$ and $C_0 = 1.21$.

Table 5 shows that data sets with excessive buoyancy forces, particularly those with either insufficient acceleration monitoring or large pipe diameters, have significantly

lower critical void fraction than the zero-g qualified data sets. The presence of such significant buoyancy forces in these data sets causes bubbles to collect at the top of a pipe and coalesce as can be seen from the Colin (1990) films. This leads to a buoyancy induced, premature transition from bubbly-to-slug.

With reference to Table 5, the unqualified Colin and Fabre (1995) 0.0190 m pipe diameter air-water data set has a critical void fraction of 0.45 which is consistent with those of the qualified data sets. This particular data set was not zero-g qualified because its buoyancy-to-surface tension force ratio was 1:7 which exceeded the 1:10 cut off. Because the critical void fraction for the 0.0190 m data set is consistent with the qualified data sets and has a reasonable buoyancy-to-surface tension ratio, the flow regime transitions were likely unaffected by buoyancy forces. Subsequently, the Colin and Fabre (1995) 0.0190 m data set should be reconsidered as representative of zero-g and used for model evaluation later in this study.

4.3.2 REPEATABILITY

The unreliability of data taken with mono-axial acceleration monitors is demonstrated in this section. The comparison of two independently collected data sets which both used tri-axial monitoring is followed by the comparison of two data sets that both used mono-axial acceleration monitoring.

The Dukler et al. (1988) and Bousman (1994) 0.0127 m diameter air-water systems both used tri-axial acceleration monitoring. With reference to Figure 15, a comparison of the data sets show excellent consistency and separation between the flow regimes, especially in the bubbly and slug regions. The two systems are very similar in design and come from the same research group. It should be observed from Figure 15 that the Dukler et al. (1988) data set does not consider the bubbly/slug flow regime and overall uses a slightly different flow regime classification system than Bousman (1994). The Dukler et

al. (1988) and Bousman (1994) experiments are suspected to have used the same mixing apparatus but this cannot be confirmed. In summary, the differences are slight and the reproducibility can be appreciated.

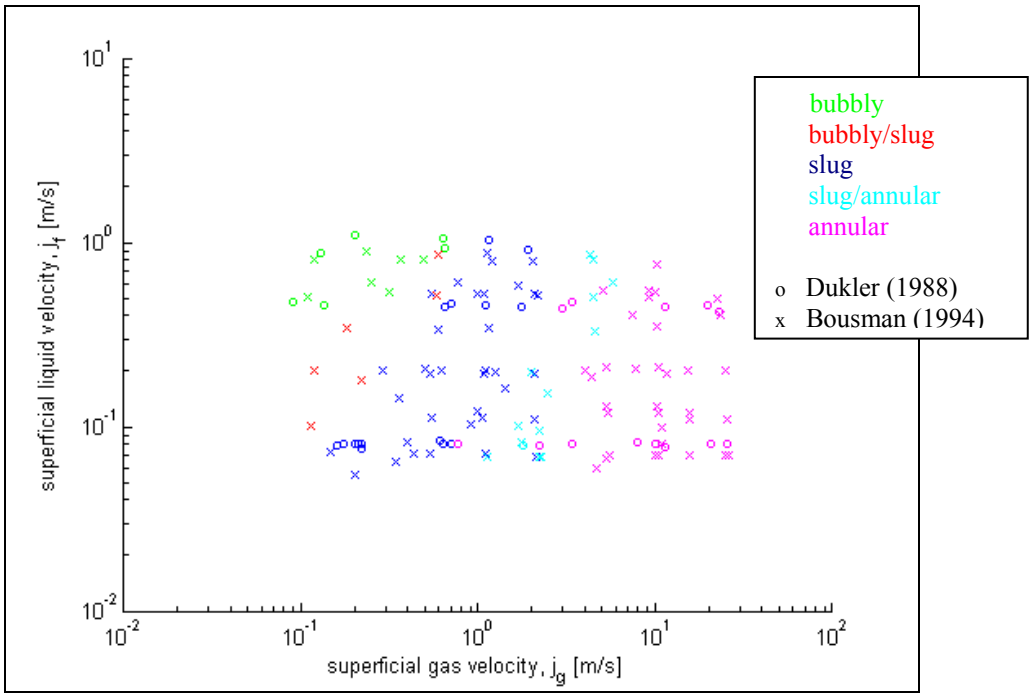

Figure 15 – Comparison of the Dukler et al. (1988) and Bousman (1994) 0.0127 m diameter air-water data sets.

The Huckerby and Rezkallah (1992) and Zhao 0.009525 m diameter air-water systems both used mono-axial acceleration monitoring. With reference to Figure 16, a comparison of the data sets show poor consistency in the separation between the flow regimes, especially in the bubbly and slug regions. The two systems are very similar in design and come from the same research group. It should be observed from Figure 16 that the Zhao and Rezkallah (1993) data set does not consider the bubbly/slug flow regime and overall uses a slightly different flow regime classification system than Huckerby and Rezkallah (1992). Also, different mixing apparatus were used for the two

experiments. It is inconclusive if the data sets are inconsistent because of buoyancy affects or because of the use of different mixing apparatus. However, the differences are appreciable and the lack of reproducibility is apparent.

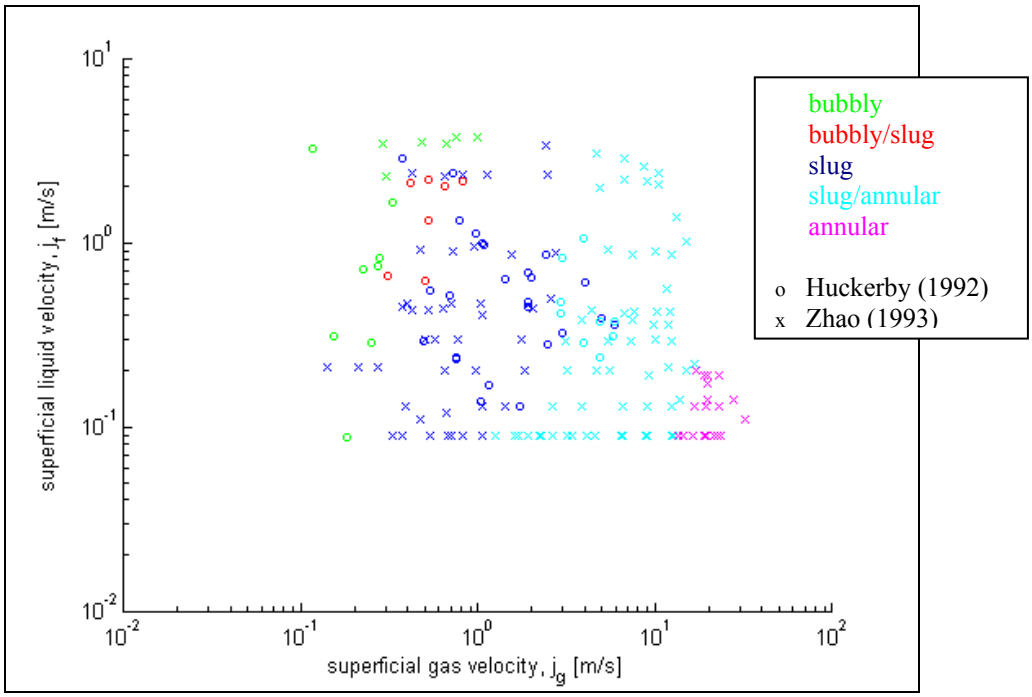

Figure 16 – Comparison of the Huckerby and Rezkallah (1992) and Zhao and Rezkallah (1993) 0.009525 m diameter air-water data sets.

In further comparison of qualified and unqualified data sets, the overlap of flow regime regions within a given data set is small for qualified data sets and large for unqualified data sets. The Colin et al. (1991) 0.0400 m diameter air-water data set (unqualified), shown in Figure 17, shows significant overlap in the flow regimes. However, the Colin and Fabre (1995) 0.0060 m diameter air-water system data set (qualified), shown in Figure 18, shows significantly less flow regime region overlap. The two systems are very similar in design and come from the same experimenter. It should be observed from Figure 17 that the Colin et al. (1991) data set does not consider the bubbly/slug

flow regime. Comparison between the two data sets demonstrates the relevance of buoyancy forces to reproducibility.

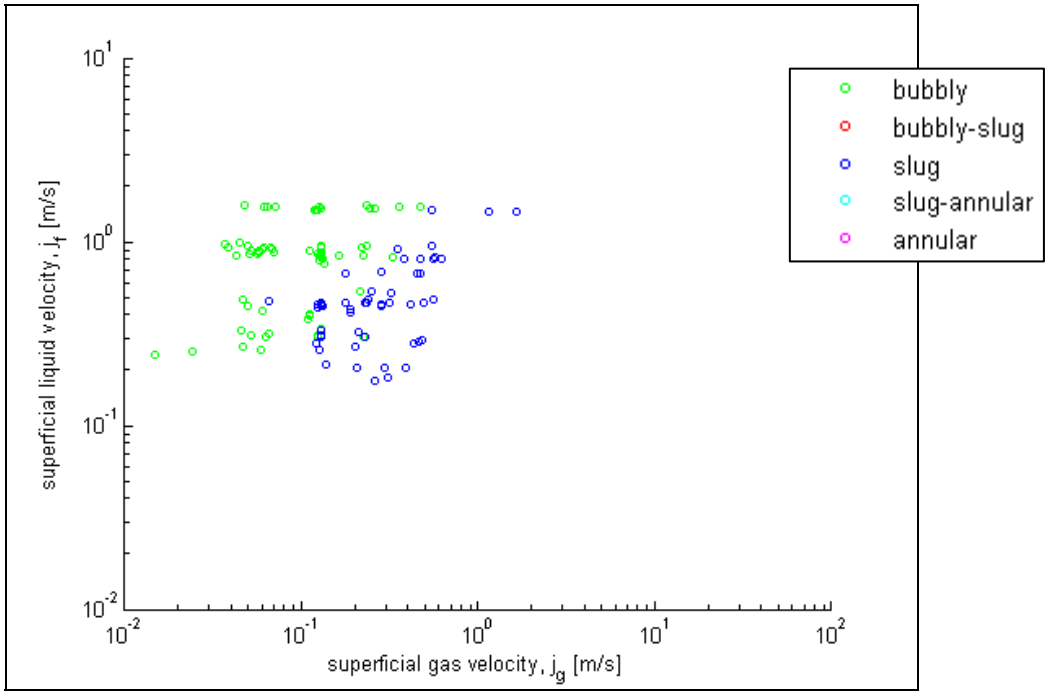

Figure 17 – Unqualified data set exhibiting significant regime overlap. Colin et al. (1991) 0.0400 m diameter air-water system.

Flow regime maps are demonstrated to be repeatable. The differences existing between the qualified and unqualified data sets are appreciable in light of repeatability. Tri-axial measurement and buoyancy limitations are necessary for producing representative zero-g data sets.

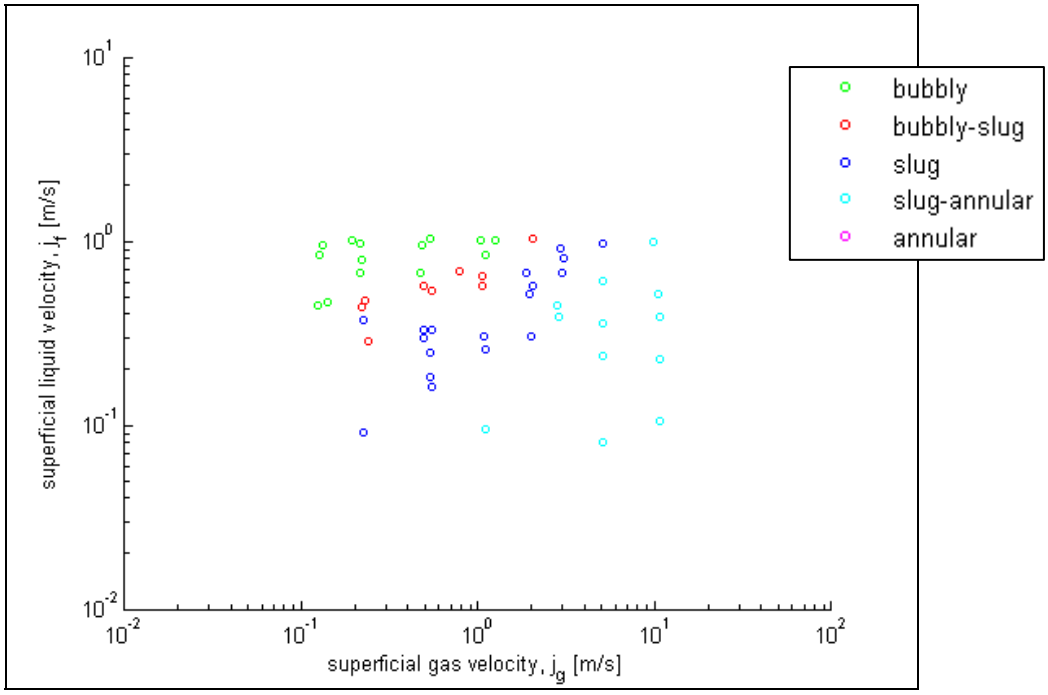

Figure 18 – Qualified data set exhibiting minimal regime overlap. Colin and Fabre (1995) 0.0060 m diameter air-water system.

4.4 SUMMARY

The data sets presented in Chapter II have been evaluated using the zero-g quality criteria developed in Chapter III. The accelerations and buoyancy forces present in several of the data sets are recognized to be too high to be representative of zero-g flows. When buoyancy forces approach the magnitude of surface tension forces, it acts to promote coalescence which leads to premature bubbly-to-slug transition. Only data sets qualified by the zero-g criteria set forth in this study will be used in the later evaluation of microgravity flow regime models with the exception of the Colin and Fabre (1995) 0.0190 m air-water system. This particular data set, while exhibiting a buoyancy-to-surface tension force ratio of 1:7, was shown to not have the buoyancy promoted coalescence that other unqualified data sets demonstrated and subsequently will be used in the evaluation of the models later in this study.

CHAPTER V
CURRENT MODELS

5.1 INTRODUCTION

In this chapter, the bubbly-slug flow regime transition models currently available in the literature are presented. These models are listed below.

- critical void fraction model (Dukler et al. 1988)
- drift-flux model (Bousman 1994)
- force balance model (Reinarts 1993)
- Suratman number correlation model (Jayawardena et al. 1997)

The critical void fraction, drift-flux, force balance models are semi-empirical while the Suratman number correlation is dimensionless correlation based on empirical data. The force balance model is specific to the slug-to-bubbly transition (not the bubbly-to-slug transition).

5.2 CRITICAL VOID FRACTION MODEL

Dukler et al. (1988) proposed the use of an empirically determined critical void fraction as an indicator of the bubbly-to-slug flow regime transition. From this foundation, the bubbly-to-slug transition would occur when bubbles coalesce to a point where they become larger than the pipe diameter. The derived model is shown below.

This model is based on the assertion that for bubbly and slug flow, there is no drift between the gas and liquid phases.

$$u_g = u_f \tag{5.1}$$

In equation (5.1), u_i is the velocity of phase *i*, and the *f* and *g* subscripts distinguish the liquid and gas properties, respectively. The liquid and gas superficial velocities are related to the liquid and gas velocities and void fraction by (5.2) and (5.3).

$$u_f = \frac{j_f}{1-\alpha_{cr}} \tag{5.2}$$

$$u_g = \frac{j_g}{\alpha_{cr}} \tag{5.3}$$

In equations (5.2) and (5.3), j_i is the superficial velocity of phase *i* and α_{cr} is the empirically determined critical void fraction. Equations (5.2) and (5.3) are then substituted into (5.1).

$$j_f = \frac{1-\alpha_{cr}}{\alpha_{cr}} j_g \tag{5.4}$$

It is noted that *this model is independent of pipe diameter and fluid properties*.

5.3 DRIFT-FLUX MODEL

Bousman (1994) proposed using the Zuber and Findlay (1965) drift-flux model to define the bubbly-to-slug transition. This model is similar to the Dukler et al. (1988) critical void fraction model except that it additionally accounts for the slower moving, entirely liquid layer along the wall by use of a distribution coefficient. As with the Dukler et al. (1988) critical void fraction model, the bubbly-to-slug transition would occur when bubbles coalesce to a point where they become larger than the pipe diameter.

$$j_f = \frac{1-C_0\alpha_{cr}}{C_0\alpha_{cr}} j_g \tag{5.5}$$

In equation (5.5), j_i is the superficial velocity for phase i, α_{cr} is the empirically determined critical void fraction, C_0 is the empirically determined distribution coefficient, and the f and g subscripts distinguish the liquid and gas properties, respectively. It is noted that *this model is independent of pipe diameter and fluid properties*.

5.4 FORCE BALANCE MODEL

Reinarts (1993) theorized the slug-to-bubbly (not the bubbly-to-slug) transition mechanism to be a force balance. The transition is modeled by the balance of the turbulence and viscous forces, which act to destroy the bubble, and the surface tension forces which act to maintain the bubble. All these forces act on the surface of the bubble.

$$p_\sigma = p_T + p_\mu \tag{5.6}$$

In equation (5.6), p_σ is the surface tension pressure , p_T is the turbulence pressure, and p_μ is the shear pressure. The expressions for the turbulent, shear, and surface tension forces are substituted for the following relations.

$$p_T = \frac{1}{2}\rho_f u_T^2 \tag{5.7}$$

$$p_\mu = \frac{1}{2} f_L \rho_f u_f^2 \tag{5.8}$$

$$p_\sigma = \frac{\sigma}{R_b} \tag{5.9}$$

In equations (5.7) through (5.9), ρ_f is the fluid density, u_T is the liquid velocity, f_L is the liquid friction factor, u_f is the liquid velocity, σ is the surface tension, and R_b is the

bubble radius. The turbulence velocity, friction faction, and bubble radius are expressed by the following relations.

$$u_T = u_f \sqrt{\frac{f_L}{2}} \tag{5.10}$$

$$f_L = 0.046 \left(\frac{\rho_f u_f D}{\mu_f} \right)^{-0.2} \tag{5.11}$$

$$R_b \sim \frac{D}{2} \tag{5.12}$$

In equations (5.11) and (5.12), μ_f is the liquid viscosity and D is the pipe diameter. Equations (5.7) through (5.12) are combined and substituted into (5.6). Then, the terms are rearranged to solve for the liquid velocity.

$$u_f = \left(\frac{\frac{2\sigma}{D}}{0.046 \cdot \frac{3}{4} \rho_f \left(\frac{\rho_f D}{\mu_f} \right)} \right)^{1/1.8} \tag{5.13}$$

The liquid superficial velocity is related to the liquid velocity and void fraction by (5.2).

$$u_f = \frac{j_f}{(1 - \alpha_{cr})} \tag{5.2}$$

In equation (5.2), j_f is the superficial liquid velocity, and α_{cr} is the empirically determined critical void fraction. The terms are rearranged to solve for the superficial liquid velocity.

$$j_f = \left(1-\alpha_{cr}\right)\left(\frac{\frac{2\sigma}{D}}{0.046\cdot\frac{3}{4}\rho_f\left(\frac{\rho_f D}{\mu_f}\right)}\right)^{1/1.8} \tag{5.14}$$

It is noted that *this model is independent of gas flow conditions.*

5.5 SURATMAN NUMBER CORRELATION MODEL

Jayawardena et al. (1997) proposed a model where the Suratman number is used to identify both the bubbly-slug and slug-annular transition. The model correlates the ratio of the superficial gas and superficial liquid Reynolds numbers and the Suratman number by use of a power law fit shown in (5.15).

$$\frac{\mathrm{Re}_g}{\mathrm{Re}_f} = K\,Su_f^{-2/3} \qquad for \quad 10^4 < Su_f < 10^7 \tag{5.15}$$

In equation (5.15), Re_f is the liquid superficial Reynolds number, Re_g is the gas superficial Reynolds number, K is the correlation coefficient, and Su_f is the liquid Suratman number. Jayawardena empirically determined the constant from available data to be that in (5.16).

$$K = 464.16 \tag{5.16}$$

The Suratman and superficial Reynolds numbers are calculated using the forms below.

$$Su_f = \frac{\mathrm{Re}_f^2}{We_f} = \frac{\left(\frac{\rho_f u_f D}{\mu_f}\right)^2}{\frac{\rho_f u_f^2 D}{\sigma}} = \frac{\sigma D \rho_f}{\mu_f^2} \tag{5.17}$$

$$\mathrm{Re}_f = \frac{\rho_f j_f D}{\mu_f} \tag{5.18}$$

$$\mathrm{Re}_g = \frac{\rho_g j_g D}{\mu_f} \tag{5.19}$$

In equations (5.17) through (5.19), u_i is the velocity for phase i, j_i is the superficial velocity for phase i, ρ_i is the density for phase i, D is the pipe diameter, μ_f is the liquid viscosity, σ is the surface tension, and the f and g subscripts distinguish the liquid and gas properties, respectively. The gas superficial Reynolds number is modified by use of the liquid viscosity term instead of the gas viscosity term to better express that bubbles do not approach the pipe wall in zero-g two-phase flow.

5.6 SUMMARY

The bubbly-slug transition models currently available in the literature were presented in this chapter. The critical void fraction, drift-flux, and force balance models are semi-empirical while the Suratman correlation model is entirely empirical. The critical void fraction, drift flux, and Suratman models are dimensionless while the force balance model is independent of gas properties and flow rates. These models will be compared against the zero-g qualified data sets in Chapter VIII.

CHAPTER VI
NEW MODELS

6.1 INTRODUCTION

The new models proposed in this thesis incorporate boundary layer and coalescence affects to mechanically explain the bubbly-to-bubbly/slug and bubbly/slug-to-slug transitions (hereon referred to as bubbly-bubbly/slug and bubbly/slug-slug transition, respectively). These transitions will additionally be shown to be dependent on the inlet bubble size distribution and hence, the mixing apparatus.

This chapter is broken up into two sections. The first section provides a conceptual overview of the phenomena which cause the bubbly-bubbly/slug and bubbly/slug-slug transitions. The second section provides the mathematical modeling of the transitions.

6.2 THEORY

This section provides a conceptual explanation of the phenomenon theorized to cause the bubbly-bubbly/slug and bubbly/slug-slug transitions.

6.2.1 VELOCITY PROFILE, WALL FRICTION, AND PRESSURE DROP

It is theorized that zero-g two-phase flow conditions near the wall can be approximated by one-g single-phase flow models. The basis for such application of one-g models is two fold. First, bubbles are not observed along the wall (Dukler et al. 1988, Colin et al. 1991, Huckerby et al. 1992, Zhao et al. 1993, Reinarts 1993, Bousman 1994, Colin et al. 1995, 1996) and thus single-phase models can be used to describe the flow near the wall. Second, zero-g two-phase pressure drop has been shown to be consistent with one-g single-phase pressure drop models (Colin et al. 1991, 1995, 1996). Based on these

findings, it appears that the interactions near the pipe wall are nearly independent of gravitational effects. As a result, one-g single-phase models for friction factor, pressure drop, wall shear, and velocity profile near the wall will be assumed accurate enough to model zero-g two-phase flow.

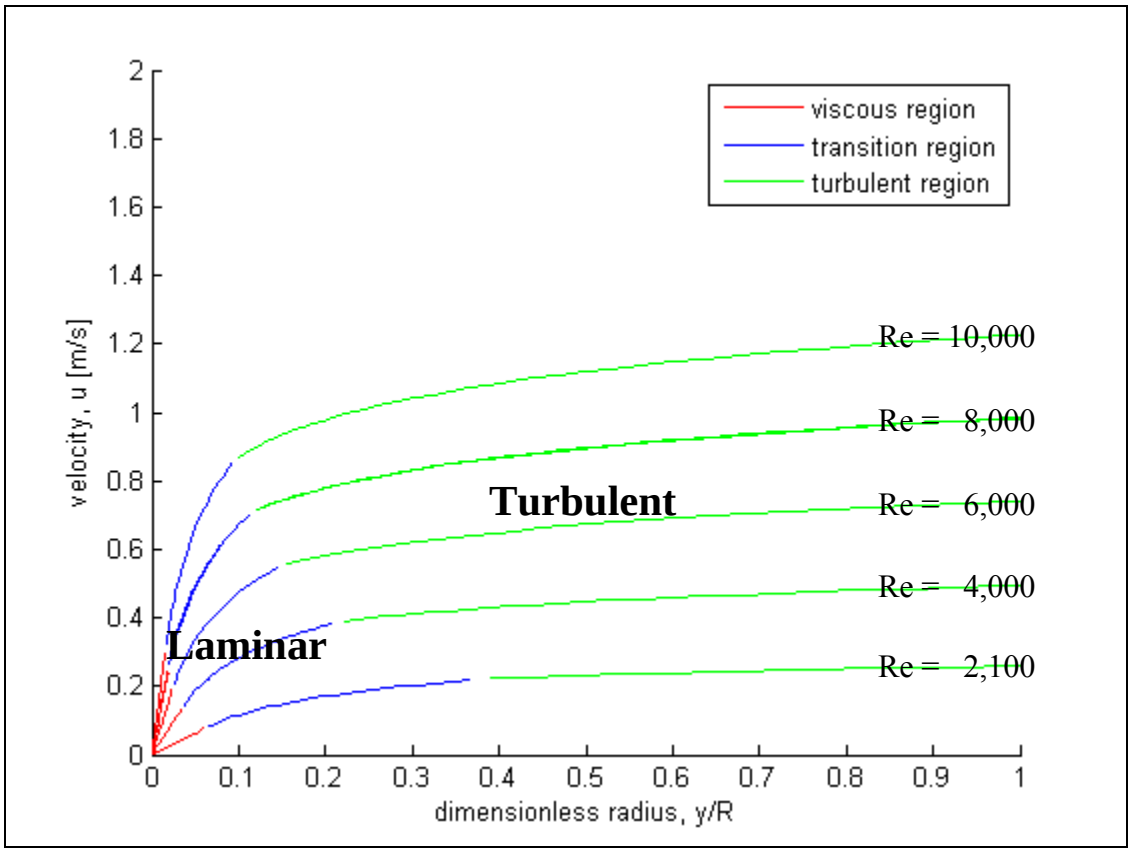

Figure 19 – Mixture velocity as a function of dimensionless radius for various Reynolds number flows for a 0.0100 m diameter pipe with water. The logarithmic velocity profile is that suggested by Lin et al. (1953).

In one-g single-phase non-laminar flow (Re > 2100) there are three flow regions that exist. Nearest the wall is a viscous sublayer region where viscous forces are dominant, and the flow is laminar. Next is a transition sublayer region where viscous and inertial forces are both dominant and the flow is laminar. Last is the center channel region

where inertial forces are dominant, turbulence eddies are present, and the time-averaged velocity profile is flat. In Figure 19, the three aforementioned regions are plotted for a range of Reynolds numbers using the logarithmic profiles suggested by Lin, Moulton, and Putnam (1953).

It is further theorized that for microgravity flows, *the laminar sublayer (the combined viscous and transition sublayer regions where the flow is laminar) creates a shear force barrier which prevents bubbles from approaching the wall*. Thus, bubbles only exist outside the laminar sublayer and inside the turbulent center channel. This theory is illustrated in Figure 20.

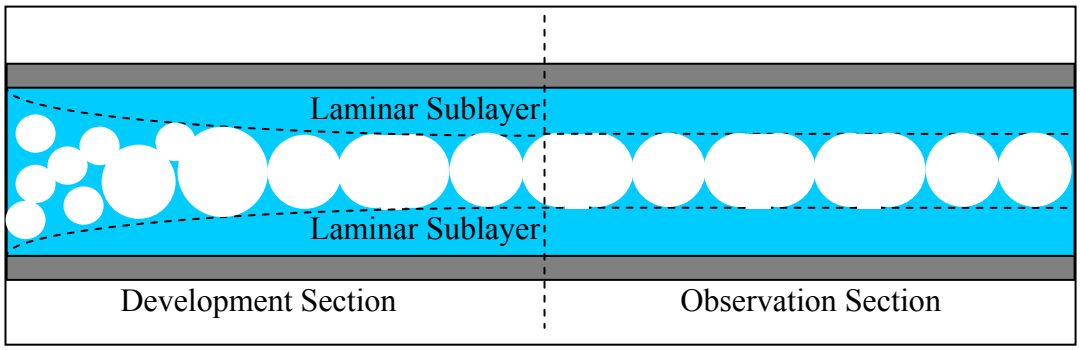

Figure 20 – Laminar sublayer affect on bubbles for microgravity flows.

It is proposed that coalescence is promoted along the development length by the reduction in the cross-sectional area outside the laminar sublayer. It is also theorized that the inlet bubble size distribution plays a significant role in determining the manner in which bubbles coalesce along the development length and the resulting fully developed flow regime.

6.2.2 COALESCENCE

Presented now is a discussion on the manner in which bubbles coalesce along the development length, beginning with a simplified example. Observed bubbles are the cumulative volumes of the smaller bubbles which coalesced to form them. Thus, there exists a discrete range of bubble sizes which can exist given a constant inlet bubble size. For example, if an inlet bubble volume was 2 mm^3 then the only possible bubble volumes would be discrete integer values of the inlet bubble volume, $2n$ mm^3, where n is the number of inlet bubbles which coalesced to form the observed bubble. This simplified example is illustrated in Figure 21.

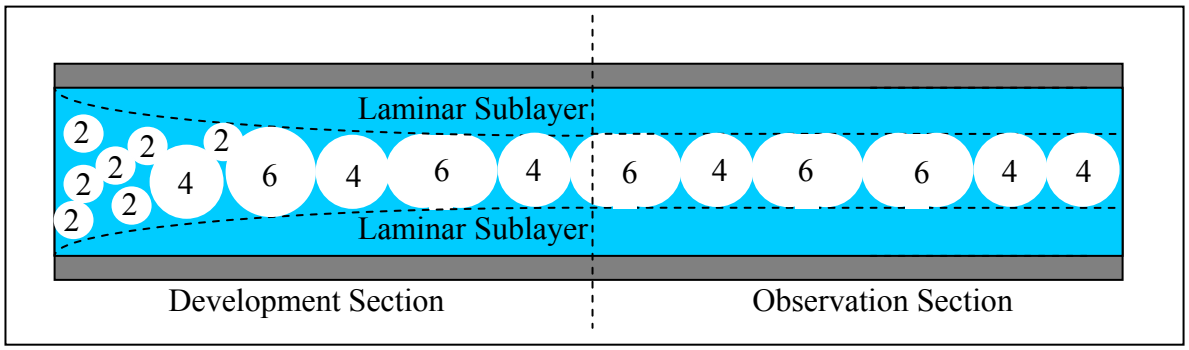

Figure 21 – Conservation of volume during coalescence.

It is understood that for real systems the inlet bubble size is not constant but exists as a distribution of sizes that varies depending on the gas and liquid flow rates and mixing apparatus. Based on this fact, a theory is extrapolated from the simplified example. When the inlet bubble size distribution is narrow and coalescence is not extensive, the resulting fully developed bubble sizes can be generalized by a discrete distribution. However, when the inlet bubble size distribution is wide or coalescence is extensive, the resulting fully developed bubbles can be generalized by a continuous distribution.

Bubble coalescence as a function of inlet bubble size distribution is examined for four simplified cases.

- Case 1: inlet bubble diameters > center channel diameter
  $D_{bubble} > D_{center\ channel}$
- Case 2: inlet bubble diameters < and > center channel diameter
  $D_{bubble} <$ and $> D_{center\ channel}$
- Case 3: inlet bubble diameters < center channel diameter
  $D_{bubble} < D_{center\ channel}$
- Case 4: inlet bubble diameters << center channel diameter
  $D_{bubble} << D_{center\ channel}$

Case 1, occurs when the inlet bubble size distribution consists of only large bubbles ($D_{bubble} > D_{center\ channel}$) and is illustrated in Figure 22. As the cross-sectional area of the center channel becomes smaller with development length, the large bubbles elongate because of the shear force barrier of the laminar sublayer. For this case, the bubbly and bubbly/slug regions are not present and thus bubbly-bubbly/slug and bubbly/slug-slug transitions are not observed.

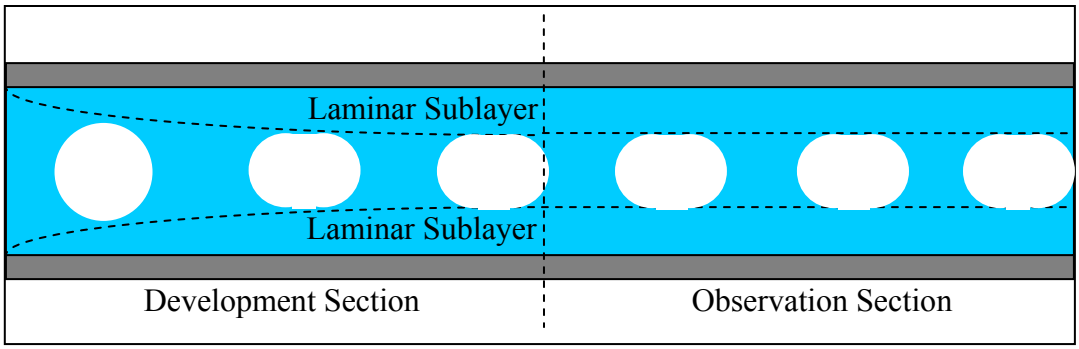

Figure 22 – Case 1: Inlet bubble sizes are large.

Case 2 occurs when the inlet bubble size distribution includes small and large bubbles (D_{bubble} < and > $D_{center\ channel}$) and is illustrated in Figure 23. As the cross-sectional area of the center channel becomes smaller with development length, the large bubbles elongate because of the shear force barrier of the laminar sublayer while the small bubbles remain spherical because they are sufficiently far from the barrier. Upon critical packing of small bubbles, they will coalesce. For this case, the bubbly regime is not observed, however the bubbly/slug regime is observed and thus the bubbly/slug-slug transition occurs. The bubbly/slug-slug transition occurs when all bubbles become critically packed in a manor which forces all the original small bubbles ($D_{bubble} < D_{center\ channel}$) to coalesce into large bubbles ($D_{bubble} > D_{center\ channel}$). For this case, coalescence and elongated bubble formation is a gradual process along the development length.

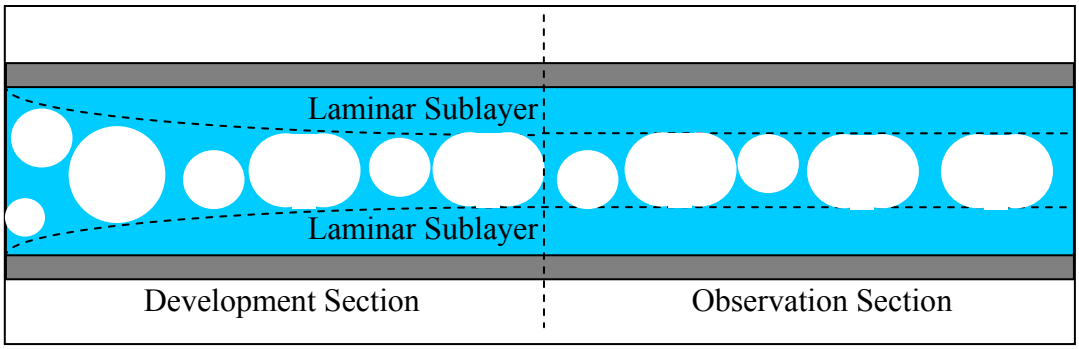

Figure 23 – Case 2: Inlet bubble sizes range from small to large.

Case 3 occurs when the inlet bubble size distribution includes only small bubbles ($D_{bubble} < D_{center\ channel}$) and is illustrated in Figure 24. As the cross-sectional area of the center channel becomes smaller with development length, the small bubbles are corralled into a tighter space, which increases the probability of two bubbles meeting and coalescing. Upon critical packing of small bubbles, they will coalesce. For this case, the bubbly and bubbly/slug regimes are observed and the bubbly-bubbly/slug and bubbly/slug-slug transitions occur. The bubbly-bubbly/slug transition occurs when coalescence is

sufficient to produce a large bubble ($D_{bubble} > D_{center\ channel}$). The bubbly/slug-slug transition occurs when all bubbles become critically packed in a manor which forces all the original small bubbles ($D_{bubble} < D_{center\ channel}$) to coalesce into large bubbles ($D_{bubble} > D_{center\ channel}$).

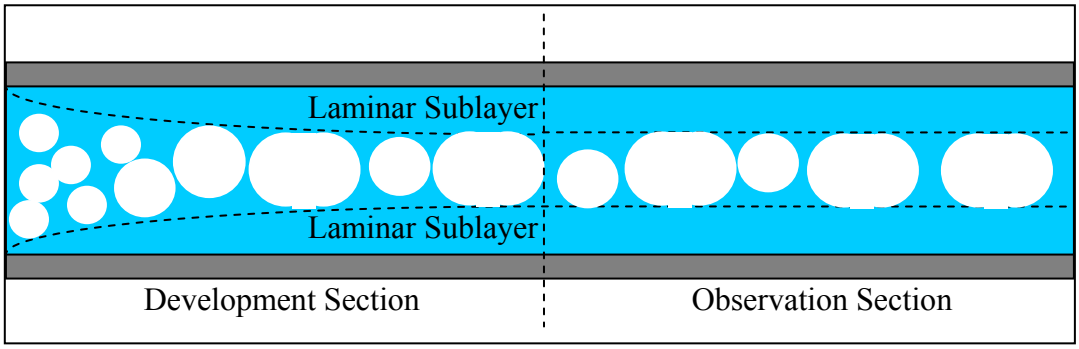

Figure 24 – Case 3: Inlet bubble sizes are small.

Case 4 occurs when an inlet bubble size distribution includes only very small bubbles ($D_{bubble} << D_{center\ channel}$) and is illustrated in Figure 25. As the cross-sectional area of the center turbulent channel becomes smaller, the very small bubbles pack together. Upon critical packing, the small bubbles will coalesce, becoming larger bubbles. With sufficient critical packing, large bubbles ($D_{bubble} > D_{center\ channel}$) are created which elongate because of the shear force of the laminar sublayer. The bubbly and bubbly/slug regime are present and the bubbly-bubbly/slug and bubbly/slug-slug transitions are observed. The transitions are the same as for Case 3, however, a greater volume of gas is required to critically pack bubbles before coalescence occurs and the transitions take place. The smallest bubbles are less likely to meet and coalesce. Many experimenters include these small dispersed bubbles as part of the slug flow regime definitions.

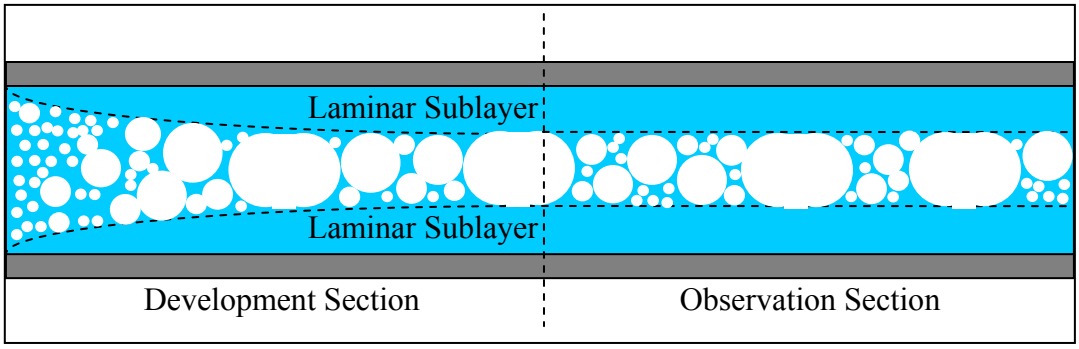

Figure 25 – Case 4: Inlet bubble sizes are very small.

In case 1, the flow regimes and their transitions are independent of coalescence effects while for cases 2, 3, and 4 they are dependent upon coalescence effects. In cases 2 and 3, the critical packing conditions which cause bubbles to coalescence are modeled differently than for case 4. The ability to discretely account for bubble sizes in cases 2 and 3 allows physical modeling to determine critical bubble packing configurations and flow regime transitions. In case 4, critical bubble packing must be modeled differently because of the continuous bubble size distribution. In summary, the bubbly-bubbly/slug and bubbly/slug-slug transitions are a function of the inlet bubble size distribution and the laminar sublayer thickness.

6.2.3 MIXING APPARATUS

The mixing apparatus used in a particular experiment determines the inlet bubble size distribution. Colin et al. (1991, 1995) used a Verturi mixer for the 0.0060, 0.0100, 0.0190, and 0.0400 m diameter air-water systems. For the 0.0400 m system, the bubble diameter at the development length inlet was measured to be 1 to 4 mm in diameter (1/40 to 1/10 the diameter of the pipe) for $(j_g, j_f) = [(0.05, 0.86), (0.06, 1.56)]$ where j_i is the superficial velocity for phase i, and the f and g subscripts distinguish the liquid and gas properties, respectively. Huckerby and Rezkallah (1992) used an injector nozzle and includes a schematic for the component. The mixing apparatus and inlet bubble size

distribution in the other data sets were not adequately described. Dukler et al. (1988)/Janicot (1988), did not specify their mixing apparatus or inlet bubble size distribution for the 0.0127 m system, however, for the 0.009525 m drop tower system it was mentioned that the "air was injected into the liquid through four peripheral holes". Bousman (1994) used an annular mixer where "the air is introduced axially into the tube while the liquid is introduced normal to the air stream…through a series of small holes evenly distributed along the internal tube." It is suspected but not confirmed that Bousman (1994) used the same mixing apparatus as the Dukler et al. (1988)/Janicot (1988) 0.0127 m system. Zhao and Rezkallah (1993) used a perforated pipe mixer where "gas enters the mixer from several small holes in the wall, and is mixed with the liquid which flows axially in the mixing chamber." Reinarts (1993) used a t-junction.

Shown in Figure 26, the anatomy of the bubbly/slug region differs for the two (or three) types of mixing apparatus used in the qualified data sets. The mixing apparatus compared here are the Venturi mixer used by Colin and Fabre (1995), the annular mixer used by Bousman (1994), and the unknown mixer used by Dukler et al. (1988) which, again, is suspected to be the same mixer used by Bousman (1994).

Upon comparison of the maps shown in Figure 26, the bubbly-bubbly/slug transitions appear similar, but the bubbly/slug-slug transitions appear different. Some of the data points in the Bousman (1994) 0.0127 m data set contrast the contour of the bubbly/slug-slug transitions in the Colin and Fabre (1995) 0.0060, 0.0100, and 0.0190 m data sets. The Dukler et al. (1988) 0.0127 data set is irresolute, lacking bubbly/slug data points.

The major difference in the mixing apparatus is that Colin and Fabre (1995) injected air into a liquid stream while Bousman (1994) injected liquid into an air stream.

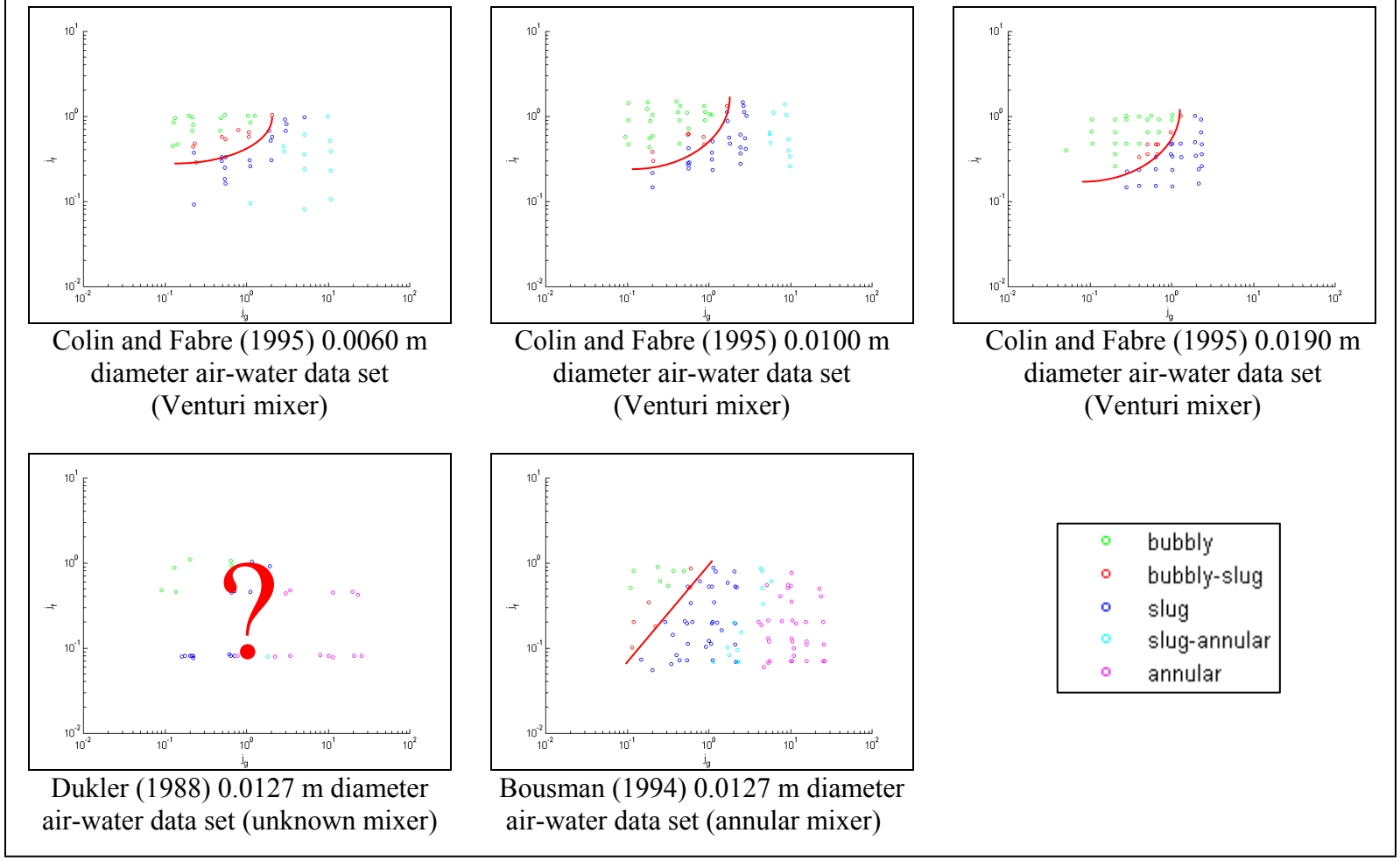

Figure 26 – Comparison of the bubbly/slug-slug transitions for different mixing apparatus.

6.2.4 ADDITIONAL CONSTRAINTS

There is a physical upper limit to both the bubbly-bubbly/slug and bubbly/slug-slug transitions. When critical bubble packing occurs in the mixing section, bubbles are physically forced to coalescence *before* entering the development length. This entirely separate coalescence phenomenon should be recognized as very different than that which takes place in the development section.

The physical upper limit for the bubbly-bubbly/slug transition occurs when coalescence in the mixing section is sufficient to output an occasional large bubble ($D_{bubble} > D_{center\ channel}$). The physical upper limit for the bubbly/slug-slug transition occurs when coalescence in the mixing section is sufficient to output only large bubbles ($D_{bubble} > D_{center\ channel}$).

The upper limits for both the bubbly-bubbly/slug and bubbly/slug-slug transitions is specific to the mixing apparatus and dependent on the component geometry, the inlet bubble size distribution to the mixer, and the flow rates. Because the mixing apparatus geometry and the inlet bubble size distributions are not available for the Dukler et al. (1988), Bousman (1994), or Colin and Fabre (1995) data sets, this upper limit can not be predicted.

6.2.5 ELONGATED BUBBLES WITH TRAILING DISPERSED BUBBLES

Elongated bubbles with trailing dispersed bubbles have been observed in the literature and are illustrated in Figure 27. Dispersed bubbles, elongated bubbles, and liquid slugs are all observed to travel at the same velocity. The dispersed bubbles are theorized to be part of the original inlet distribution of bubbles and because of their small size could “hide” in regions which did not encounter critical packing against other bubbles.

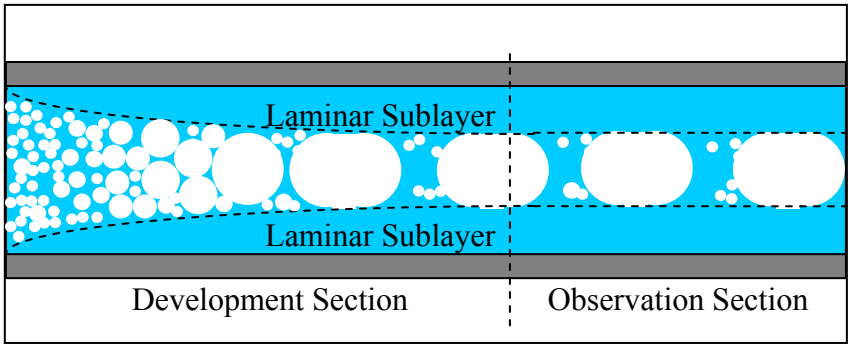

Figure 27 – Elongated bubbles with trailing dispersed bubbles.

6.3 MATHEMATICAL MODEL

This section mathematically models the bubbly-bubbly/slug and bubbly/slug-slug transitions. These models follow the concepts introduced in the previous section.

6.3.1 VELOCITY PROFILE, WALL FRICTION, AND PRESSURE DROP

The logarithmic velocity profile suggested by Lin et al. (1953) for one-g single-phase flow is applied to zero-g two-phase flow.

$$u^+ = y^+ \qquad y^+ < 5 \qquad \textit{viscous region} \qquad (6.1)$$

$$u^+ = -3.05 + 5.00 \ln\left(y^+\right) \qquad 5 < y^+ < 30 \qquad \textit{transition region} \qquad (6.2)$$

$$u^+ = 5.5 + 2.5 \ln\left(y^+\right) \qquad y^+ > 30 \qquad \textit{turbulent region} \qquad (6.3)$$

In equations (6.1) through (6.3), u^+ is the dimensionless velocity and y^+ is the dimensionless distance from the wall. These dimensionless parameters are expressed by the relationships in (6.4) and (6.5).

$$y^+ = y\frac{\sqrt{\tau_w / \rho_f}}{\mu_f / \rho_f} \tag{6.4}$$

$$u^+ = \frac{u}{\sqrt{\tau_w / \rho_f}} \tag{6.5}$$

In equations (6.4) and (6.5), τ_w is wall shear, μ_f is liquid viscosity, ρ_f is liquid density, and u is liquid velocity. Because the laminar sublayer is entirely liquid, the relation of laminar sublayer thickness is expressed as a function of liquid properties. The laminar sublayer thickness can be derived in terms of the Reynolds number. This derivation begins by solving (6.4) for distance from the wall.

$$y = y^+ \frac{\mu_f}{\rho_f}\sqrt{\frac{\rho_f}{\tau_w}} \tag{6.6}$$

The dimensionless laminar sublayer thickness can be identified from equations (6.1) through (6.3) to be that shown in (6.7). The dimensionless distance from the wall is set equal to the dimensionless laminar sublayer thickness. The dimensionless laminar sublayer thickness encompasses both the viscous and transition regions.

$$y^* = y^+ = 30 \tag{6.7}$$

In equation (6.7), y^* is the dimensionless constant corresponding to the laminar sublayer thickness. Equation (6.7) is substituted into (6.6).

$$y = y^* \frac{\mu_f}{\rho_f}\sqrt{\frac{\rho_f}{\tau_w}} \tag{6.8}$$

The wall shear is calculated using (6.9).

$$\tau_w = \frac{D}{4}\left(\frac{\Delta p}{\Delta z}\right) = \frac{f}{4}\frac{\rho_f u^2}{2} \tag{6.9}$$

In equation (6.9), D is the pipe diameter, $\Delta\rho/\Delta z$ is the pressure drop, and f is the friction factor. Equation (6.9) is substituted into (6.8) and simplified.

$$y = y^* \frac{\mu_f}{\rho_f}\sqrt{\frac{\rho_f}{\frac{f}{4}\frac{\rho_f u^2}{2}}} = y^* \frac{\mu_f}{\rho_f}\sqrt{\frac{8}{fu^2}} \tag{6.10}$$

The general relationship for the friction factor and velocity in terms of the Reynolds number is shown in (6.11) and (6.12), respectively.

$$f = C\,\mathrm{Re}^{-n} \tag{6.11}$$

$$u = \frac{\mu_f\,\mathrm{Re}}{\rho_f D} \tag{6.12}$$

In equations (6.11) and (6.12), C and n are the friction factor coefficients, and Re is the Reynolds number. Equation (6.11) and (6.12) are substituted into (6.10) and simplified.

$$y = y^* \frac{\mu_f}{\rho_f}\sqrt{\frac{8}{\left(C\,\mathrm{Re}^{-n}\right)\left(\frac{\mu_f\,\mathrm{Re}}{\rho_f D}\right)^2}} = y^* D\,\mathrm{Re}^{n/2-1}\sqrt{\frac{8}{C}} \tag{6.13}$$

Equation (6.13) is made dimensionless by dividing by the pipe radius and simplifying.

$$\frac{y}{R} = \frac{y^* D \,\mathrm{Re}^{n/2-1} \sqrt{\frac{8}{C}}}{\frac{D}{2}} = y^* \,\mathrm{Re}^{n/2-1} \sqrt{\frac{32}{C}} \tag{6.14}$$

The friction factor coefficients, C and n, are evaluated using the criteria below.

not applicable to this model	$\mathrm{Re} < 2100$	(6.15)
$C = 0.316, n = 0.25$	$2100 < \mathrm{Re} < 30000$	(6.16)
$C = 0.184, n = 0.20$	$\mathrm{Re} > 30000$	(6.17)

Restated, the dimensionless laminar sublayer thickness, y^*, is evaluated as shown below.

$y^* = 30$	*laminar sublayer thickness*	(6.18)

Using the above friction factor coefficients, the dimensionless laminar sublayer thickness, *y/R*, has an inverse relation to the Reynolds number, as expected.

A similar derivation gives the dimensionless laminar sublayer thickness as a function of pressure drop.

$$\frac{y}{R} = 4y^+ \frac{\mu_f}{\rho_f D} \sqrt{\frac{\rho_f}{\frac{D}{4}\left(\frac{\Delta p}{\Delta z}\right)}} = 4y^+ \sqrt{\frac{\mu_f^2}{\rho_f D^3 \left(\frac{\Delta p}{\Delta z}\right)}} \tag{6.19}$$

6.3.2 BUBBLY-BUBBLY/SLUG AND BUBBLY/SLUG-SLUG TRANSITION CONDITIONS

The critical bubbly-bubbly/slug configuration for inlet bubble sizes that are small ($D_{bubble} < D_{center\ channel}$) is modeled as a critical packing of bubbles with a diameter equal to that of the center channel. The configuration is shown in Figure 28.

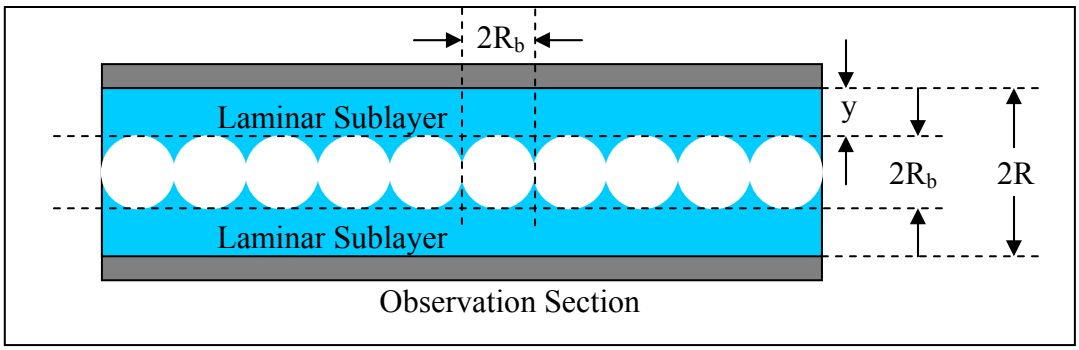

Figure 28 – Configuration used in bubbly/slug-slug transition model.

The geometric relation between the laminar sublayer thickness and the critical void fraction is determined from Figure 28 and is shown in (6.20).

$$\langle \beta_{B-B/S} \rangle = \frac{bubble\,volume}{pipe\,volume} = \frac{4/3\,\pi R_b^3}{\pi R^2 2R_b} = \frac{4/3\,\pi (R-y)^3}{\pi R^2 2(R-y)} = \frac{2}{3}\left(1-\frac{y}{R}\right)^2 \qquad (6.20)$$

The bubbly/slug-slug transition is modeled for two separate cases. The first case is for inlet bubble sizes that are small ($D_{bubble} < D_{center\ channel}$) and the second case for inlet bubble sizes that are very small ($D_{bubble} << D_{center\ channel}$).

For inlet bubble sizes that are small ($D_{bubble} < D_{center\ channel}$), the critical bubbly/slug-slug configuration is modeled such that the observed bubbles are equal in volume to two

spherical bubbles with diameters equal to the center channel. This configuration is illustrated in Figure 29.

$$2 \cdot \frac{4}{3}\pi R_b^3 = \frac{4}{3}\pi R_b^3 + \pi R_b^2 \left(L_b - 2R_b\right) \tag{6.21}$$

Equation (6.21) is solved for bubble length.

$$L_b = \frac{10}{3} R_b = \frac{10}{3}\left(R - y\right) \tag{6.22}$$

Where L_b is the bubble length, R_b is the bubble radius, y is the laminar sublayer thickness, and R is the pipe radius.

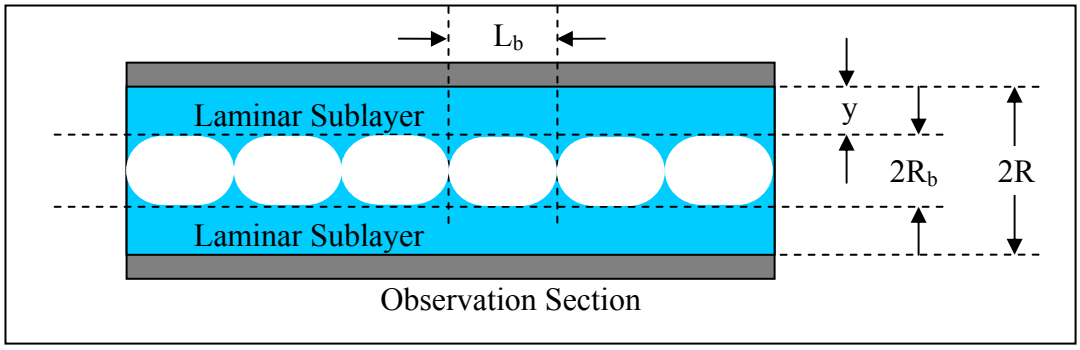

Figure 29 – Configuration used in bubbly/slug-slug transition model for small bubbles.

The bubbly/slug-slug transition for small bubbles is then defined by the geometry in Figure 29.

$$\left\langle \beta_{B/S-S} \right\rangle = \frac{bubble\,volume}{pipe\,volume} = \frac{2 \cdot 4/3\,\pi R_b^3}{\pi R^2 L_b} = \frac{2 \cdot 4/3\,\pi \left(R - y\right)^3}{\pi R^2 \cdot 10/3\left(R - y\right)} = \frac{4}{5}\left(1 - \frac{y}{R}\right)^2 \tag{6.23}$$

For inlet bubbles sizes that are very small ($D_{bubble} << D_{center\ channel}$) the theoretical bubbly/slug-slug transition upper limit can be modeled by simply assuming that the very small bubbles will be present until the center channel is completely filled with gas.

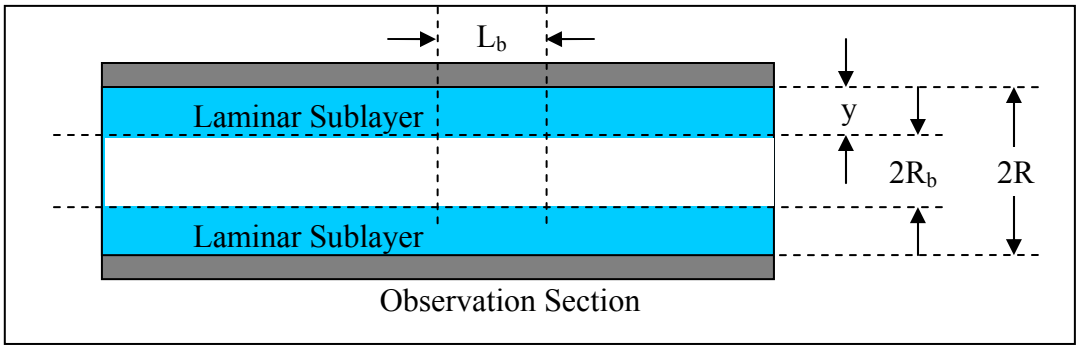

Figure 30 – Configuration used in bubbly/slug-slug transition model for very small bubbles.

The theoretical bubbly/slug-slug upper limit for the case of very small inlet bubble diameters is then defined by the geometry in Figure 30.

$$\max\left(\left\langle \beta_{B/S-S} \right\rangle\right) = \frac{bubble\,volume}{pipe\,volume} = \frac{\pi R_b^2 L_b}{\pi R^2 L_b} = \frac{\left(R-y\right)^2}{R^2} = \left(1-\frac{y}{R}\right)^2 \tag{6.24}$$

The bubbly-bubbly/slug and bubbly/slug-slug transition geometries are represented by a volumetric critical void fraction. A fundamental form is recognized from the volumetric critical void fraction equations (6.20), (6.23), and (6.24) and is presented in (6.25).

$$\left\langle \beta_{gas/total} \right\rangle = \left\langle \beta_{gas/center\ channel} \right\rangle \left\langle \beta_{center\ channel/total} \right\rangle \tag{6.25}$$

In equation (6.25), $\beta_{gas/total}$ is the ratio of the gas volume to the total pipe volume, $\beta_{gas/center\ channel}$ is the ratio of the gas volume to the center channel volume, and

$\beta_{center\ channel/total}$ is the ratio of the average gas volume to the total pipe volume. It is identified that $\beta_{gas/center}$ represents a bubble packing factor, similar to the atomic packing factor of crystalline structures. Further, $\beta_{gas/total}$ is identified as a separable function where $\beta_{center\ channel/total}$ is only a function of the Reynolds number and $\beta_{gas/center\ channel}$ is only a function the inlet bubble size distribution.

6.3.3 BUBBLY-BUBBLY/SLUG AND BUBBLY/SLUG-SLUG MODEL

The new model initially follows the Dukler et al. (1988) critical void fraction model which is re-derived here for continuity. The Dukler critical void fraction model derivation begins with the assertion that bubbles and liquid flow at the same velocity.

$$u_g = u_f \tag{5.1}$$

In equation (5.1), u_i is the velocity of phase i, and the f and g subscripts distinguish the liquid and gas properties, respectively. The phase velocity is related to the superficial velocity and the critical void fraction.

$$u_g = \langle \alpha \rangle j_g \tag{6.26}$$

$$u_f = \left(1 - \langle \alpha \rangle\right) j_f \tag{6.27}$$

In equations (6.26) and (6.27), $\langle \alpha \rangle$ is the cross-section averaged void fraction, and j_i is the superficial velocity of phase i. Equations (6.26) and (6.27) are substituted into (6.28).

$$\langle \alpha \rangle j_g = \left(1 - \langle \alpha \rangle\right) j_f \tag{6.28}$$

Equation (6.28) is solved for the superficial gas velocity.

$$j_g = \frac{\left(1-\langle\alpha\rangle\right)}{\langle\alpha\rangle} j_f \tag{6.29}$$

Because of the observed slip ratio is unity for zero-g two-phase systems, the volume averaged void fraction is equal to the cross-section averaged void fraction.

$$\langle\alpha\rangle = \langle\beta\rangle \qquad \textit{no slip condition} \tag{6.30}$$

In equation (6.30), $\langle\beta\rangle$ is the volume averaged void fraction. The cross-section averaged void fraction is thus equal to the volume averaged void fraction relationships for the bubbly-bubbly/slug and bubbly/slug-slug transitions.

$$\langle \alpha_{B-B/S} \rangle = \langle \beta_{B-B/S} \rangle = \frac{2}{3}\left(1-\frac{y}{R}\right)^2 \qquad D_{bubbles} < D_{center\ channel} \tag{6.31}$$

$$\langle \alpha_{B/S-S} \rangle = \langle \beta_{B/S-S} \rangle = \frac{4}{5}\left(1-\frac{y}{R}\right)^2 \qquad D_{bubbles} < D_{center\ channel} \tag{6.32}$$

$$\max\langle \alpha_{B/S-S} \rangle = \max\langle \beta_{B/S-S} \rangle = \left(1-\frac{y}{R}\right)^2 \qquad D_{bubbles} << D_{center\ channel} \tag{6.33}$$

The dimensionless laminar sublayer thickness was derived earlier and is reproduced here.

$$\frac{y}{R} = y^* \,\mathrm{Re}^{n/2-1} \sqrt{\frac{32}{C}} \tag{6.34}$$

Substitute (6.34) into (6.31), (6.32), and (6.33) to arrive at (6.35), (6.36), and (6.37).

$$\left\langle \alpha_{B-B/S} \right\rangle = \frac{2}{3}\left(1 - y^* \,\mathrm{Re}^{n/2-1}\sqrt{\frac{32}{C}}\right)^2 \tag{6.35}$$

$$\left\langle \alpha_{B-B/S} \right\rangle = \frac{4}{5}\left(1 - y^* \,\mathrm{Re}^{n/2-1}\sqrt{\frac{32}{C}}\right)^2 \tag{6.36}$$

$$\max\left(\left\langle \alpha_{B-B/S} \right\rangle\right) = \left(1 - y^* \,\mathrm{Re}^{n/2-1}\sqrt{\frac{32}{C}}\right)^2 \tag{6.37}$$

The Reynolds number is defined in (6.38).

$$\mathrm{Re} = \frac{(\rho u)_m D}{\mu_f} = \frac{(\rho j)_m D}{\mu_f} = \frac{\left(\rho_f j_f + \rho_g j_g\right) D}{\mu_f} = \frac{\rho_f j_f D}{\mu_f} + \frac{\rho_g j_g D}{\mu_f} = \mathrm{Re}_f + \mathrm{Re}_g \tag{6.38}$$

The liquid viscosity is used in the superficial gas Reynolds number formula because in zero-g two-phase flows, gases do not come in contact with the pipe wall. The gas component of the two-phase Reynolds number is relatively smaller than the liquid component for the bubbly, bubbly/slug, and slug regimes. Thus, the mixture Reynolds number can be approximated by the superficial liquid Reynolds number.

$$\mathrm{Re} \approx \mathrm{Re}_f = \frac{\rho_f j_f D}{\mu_f} \qquad\qquad \mathrm{Re}_f >> \mathrm{Re}_g \tag{6.39}$$

When the model is evaluated, the bubbly-bubbly/slug transition is defined as (6.40).

$$j_g = \left(\left(0.816 - 247\,\mathrm{Re}^{-0.875}\right)^{-2} - 1\right)^{-1} j_f \qquad\qquad D_{bubbles} < D_{center\ channel} \tag{6.40}$$

The bubbly/slug-slug transition is defined as (6.41) and (6.42).

$$j_g = \left(\left(0.894 - 270\,\mathrm{Re}^{-0.875} \right)^{-2} - 1 \right)^{-1} j_f \qquad D_{bubbles} < D_{center\ channel} \tag{6.41}$$

$$j_g = \left(\left(1 - 302\,\mathrm{Re}^{-0.875} \right)^{-2} - 1 \right)^{-1} j_f \qquad D_{bubbles} << D_{center\ channel} \tag{6.42}$$

6.3.4 ADDITIONAL CONSTRAINTS

The bubble packing term in the model, $\beta_{gas/center\ channel}$, has an upper limit. The critical bubble packing term is referenced from (6.25) and reproduced below.

$$\left\langle \beta_{gas/total} \right\rangle = \left\langle \beta_{gas/center\ channel} \right\rangle \left\langle \beta_{center\ channel/total} \right\rangle \tag{6.25}$$

This upper limit is modeled by critical packing configurations which upon any further packing would force a flow regime transition. This upper limit is specific to a given system and can not be accurately modeled without specific information regarding the mixing apparatus and the inlet bubble size distribution.

An example of one possible upper limit for the bubbly-bubbly/slug transition is the simple cubic critical packing, as originally suggested by Dukler et al. (1988).

$$\max\left(\left\langle \beta_{gas/center\ channel} \right\rangle \right) = \frac{bubble\,volume}{cell\,volume} = \frac{4/3\,\pi R_b^3}{\left(2R_b \right)^3} = 0.524 \tag{6.43}$$

Another example would be the body-centered critical packing for higher surface tension fluids.

$$\max\left(\left\langle \beta_{gas/center\ channel} \right\rangle \right) = \frac{\#bubbles \cdot bubble\,volume}{cell\,volume} = \frac{2 \cdot 4/3\,\pi R_b^3}{\left(4R_b / \sqrt{3} \right)^3} = 0.680 \tag{6.44}$$

These are suggested for illustrative purposes and do not pertain to a specific experiment. For systems with infinitely small inlet bubbles, there would be no critical packing upper limit.

6.4 SUMMARY

The laminar sublayer effectively creates a shear force barrier which restricts bubbles exclusively to the center channel of the flow. As the cross-sectional area of the center channel decreases with passing development length, bubbles are packed tighter and tighter. Eventually bubbles are packed tight enough where they meet and coalesce. A critical void fraction adequately describes the point of critical bubble packing. The critical void fraction is described as a function of laminar sublayer thickness. Because the laminar sublayer thickness is a function of the Reynolds number, the critical void fraction is also expressed as a function of the Reynolds number. Thus, the models presented in this chapter are purely physical and dimensionless.

The bubbly-bubbly/slug and bubbly/slug-slug transitions are dependent on the bubble size distribution at the inlet to the development section. The inlet bubble size distribution is dependent on the mixing apparatus and the gas and liquid flow rates.

The transition models are based on an assumption that zero-g two-phase flow near the pipe wall can aptly be approximated by one-g single phase models. This assumption is additionally supported by other studies.

CHAPTER VII
MODEL EVALUATION

7.1 INTRODUCTION

The zero-g qualified data sets from Chapter IV are used to evaluate the current models presented Chapter V and the new models presented in Chapter VI. While the Colin and Fabre (1995) 0.0190 m pipe diameter air-water system did not meet the zero-g qualification criteria from Chapter III, the evaluation in Chapter IV showed the data set to be characteristically similar to the qualified data sets. For this reason, the Colin and Fabre (1995) 0.0190 m data set is included in the model evaluation.

7.2 PLOTS

The plots shown in Figure 31 through Figure 35 demonstrate the models mentioned in this study and show the applicability of the existing and new models. In each plot, the Re = 2,100 and Re = 10,000 lines are included and define the onset of turbulence and fully developed turbulent flow, respectively. The Fr = 2.6 line is also included on the model plots. All points below the Fr = 2.6 line are not assumed accurate because the buoyancy-to-inertia force ratio is greater than 1:10.

7.3 COMPARISON

The critical void fraction, drift-flux, and Suratman number models are adequate in loosely defining the bubbly-slug transition. Because the bubbly-slug transition is a loose approximation which lies between the bubbly-bubbly/slug and bubbly/slug-slug transitions, these models are at best useful as a rule of thumb.

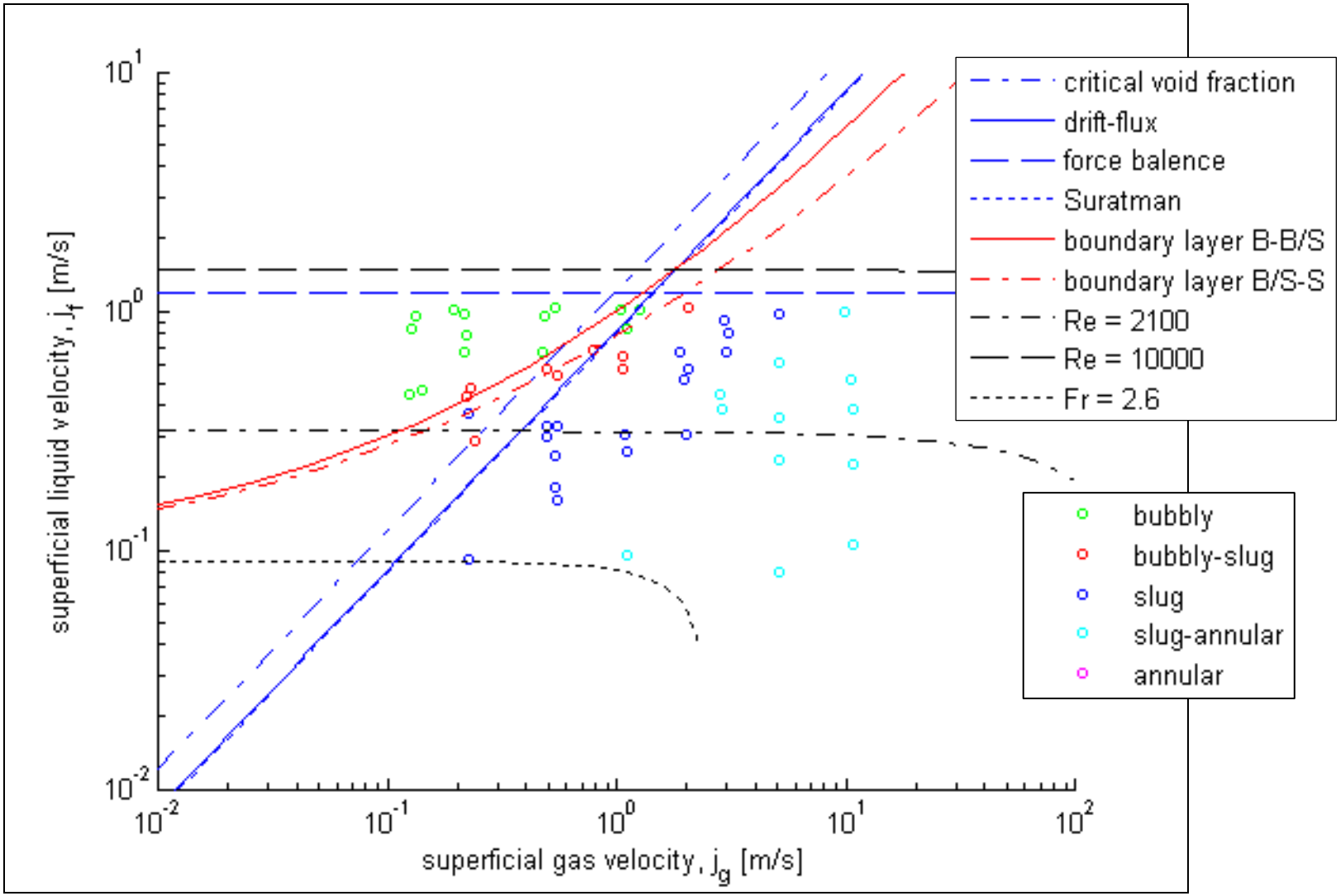

Figure 31 – Colin and Fabre (1995) 0.0060 m diameter air-water data set with models.

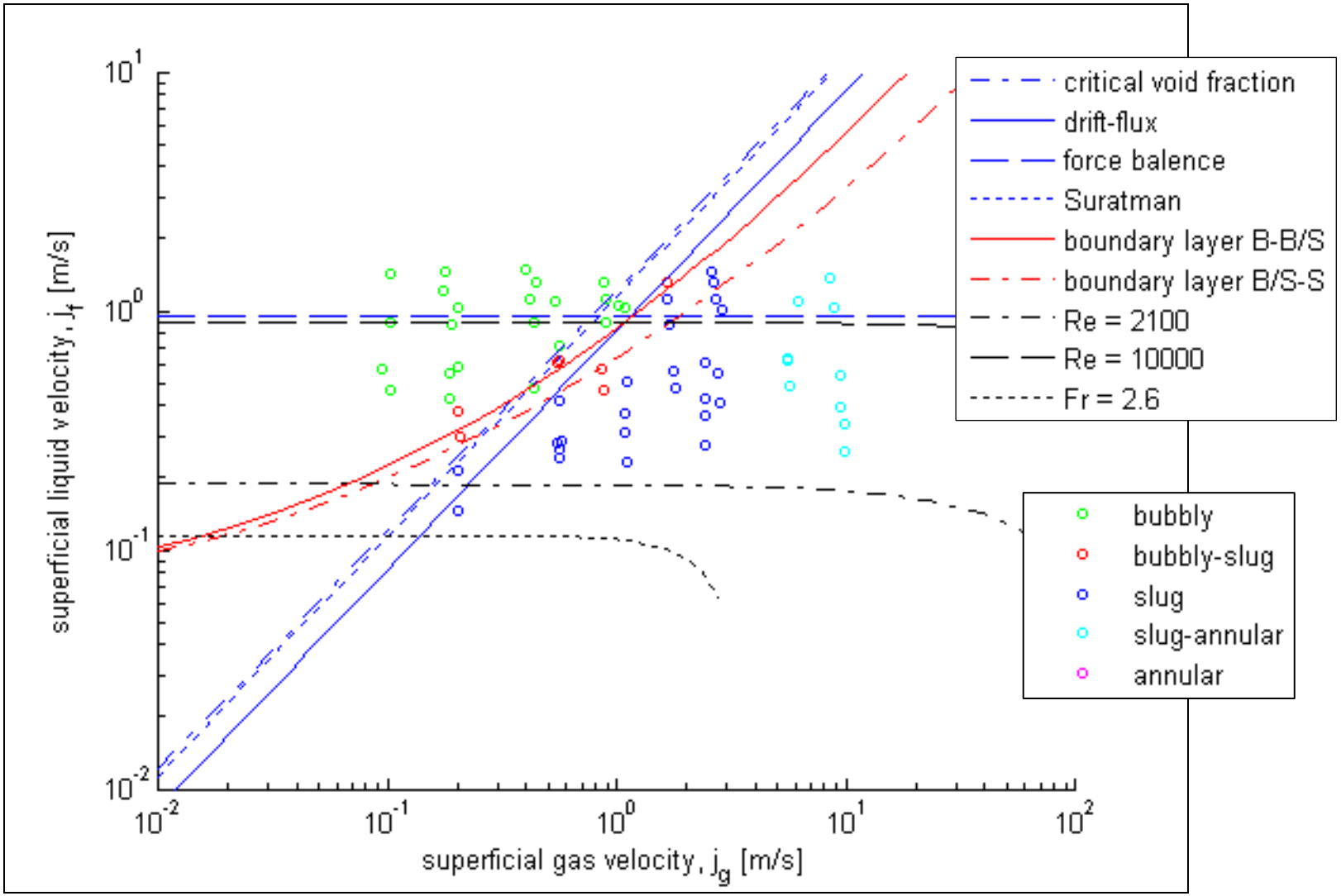

Figure 32 – Colin and Fabre (1995) 0.0100 m diameter air-water data set with models.

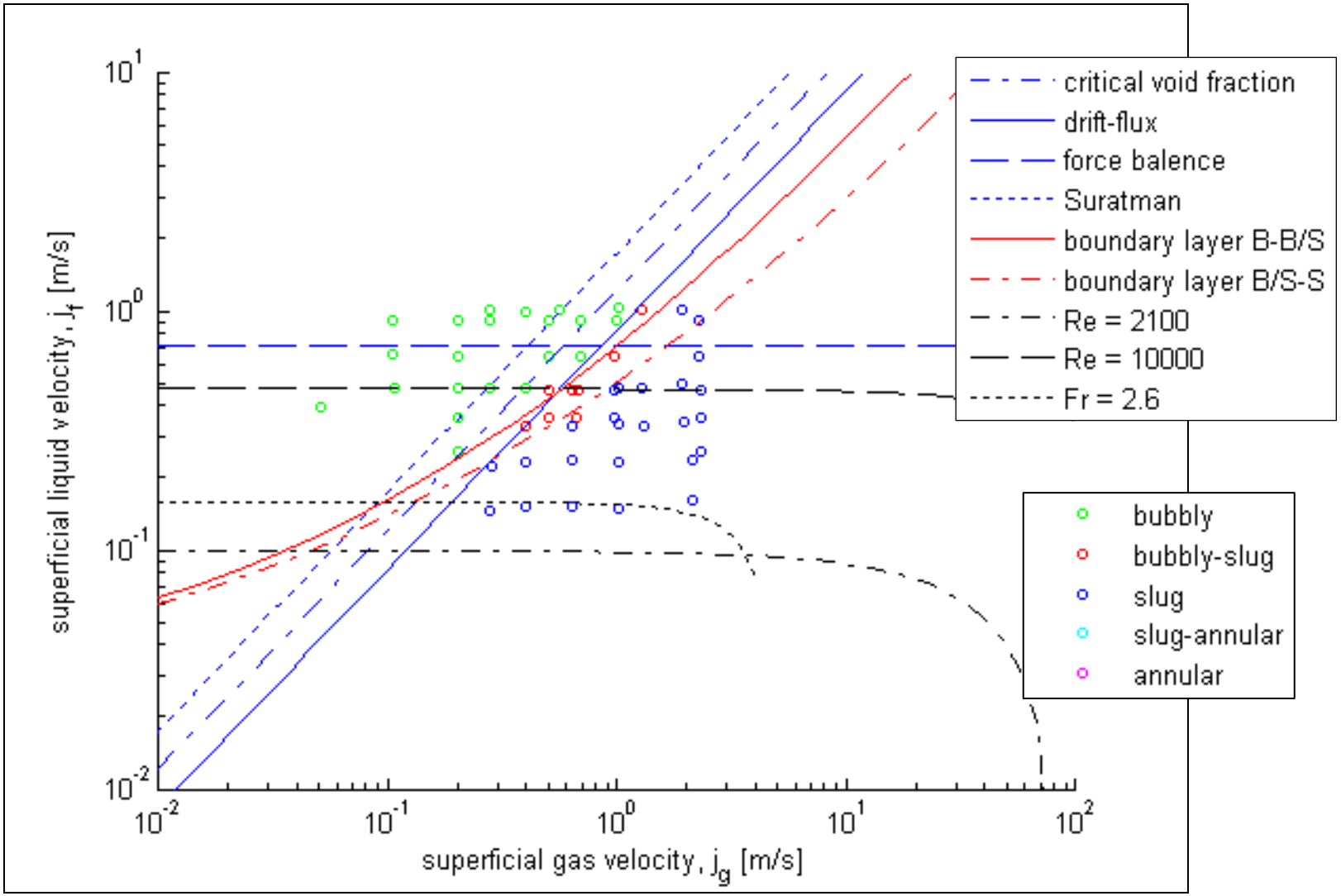

Figure 33 – Colin and Fabre (1995) 0.0190 m diameter air-water data set with models.

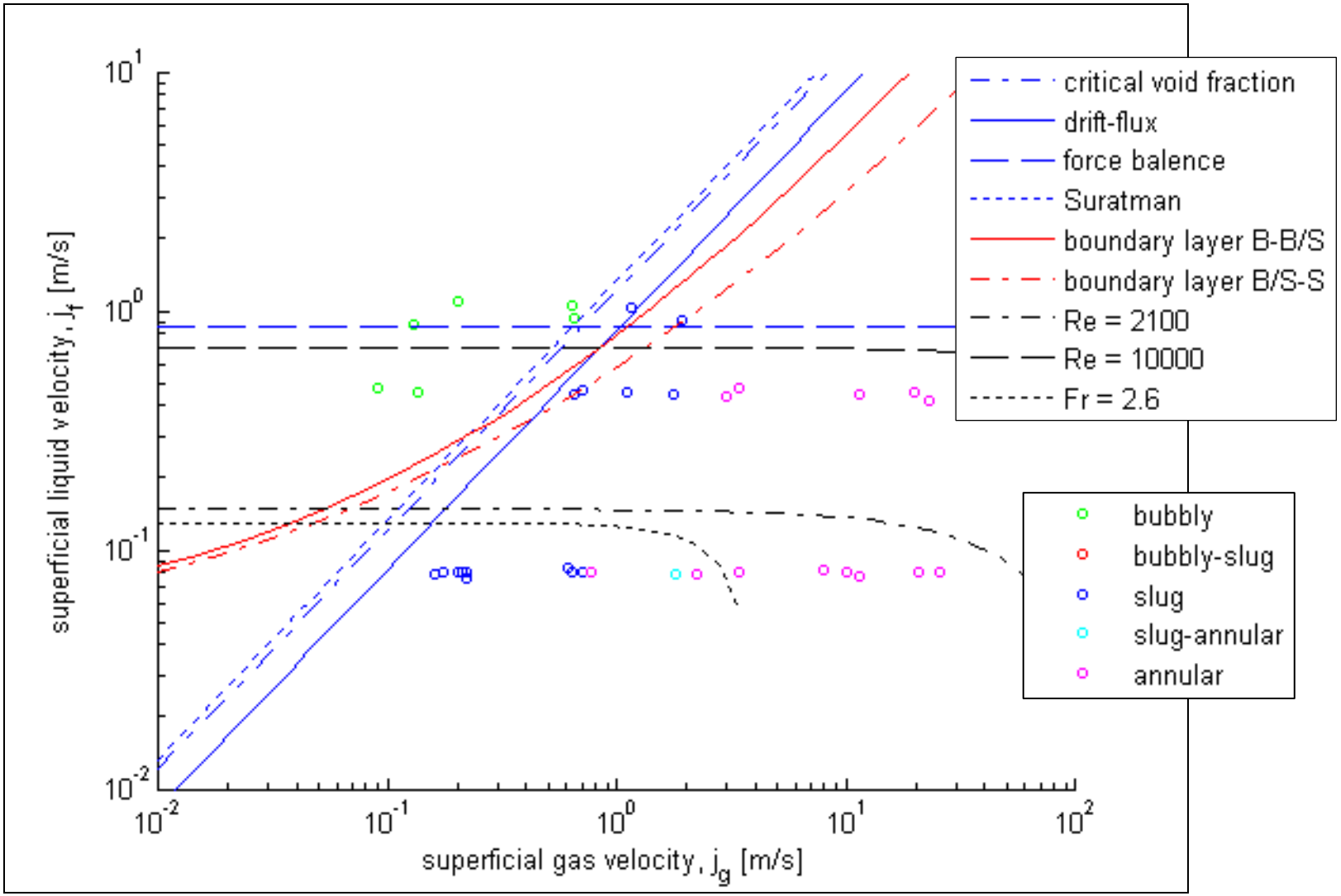

Figure 34 – Dukler et al. (1988) 0.0127 m diameter air-water data set with models.

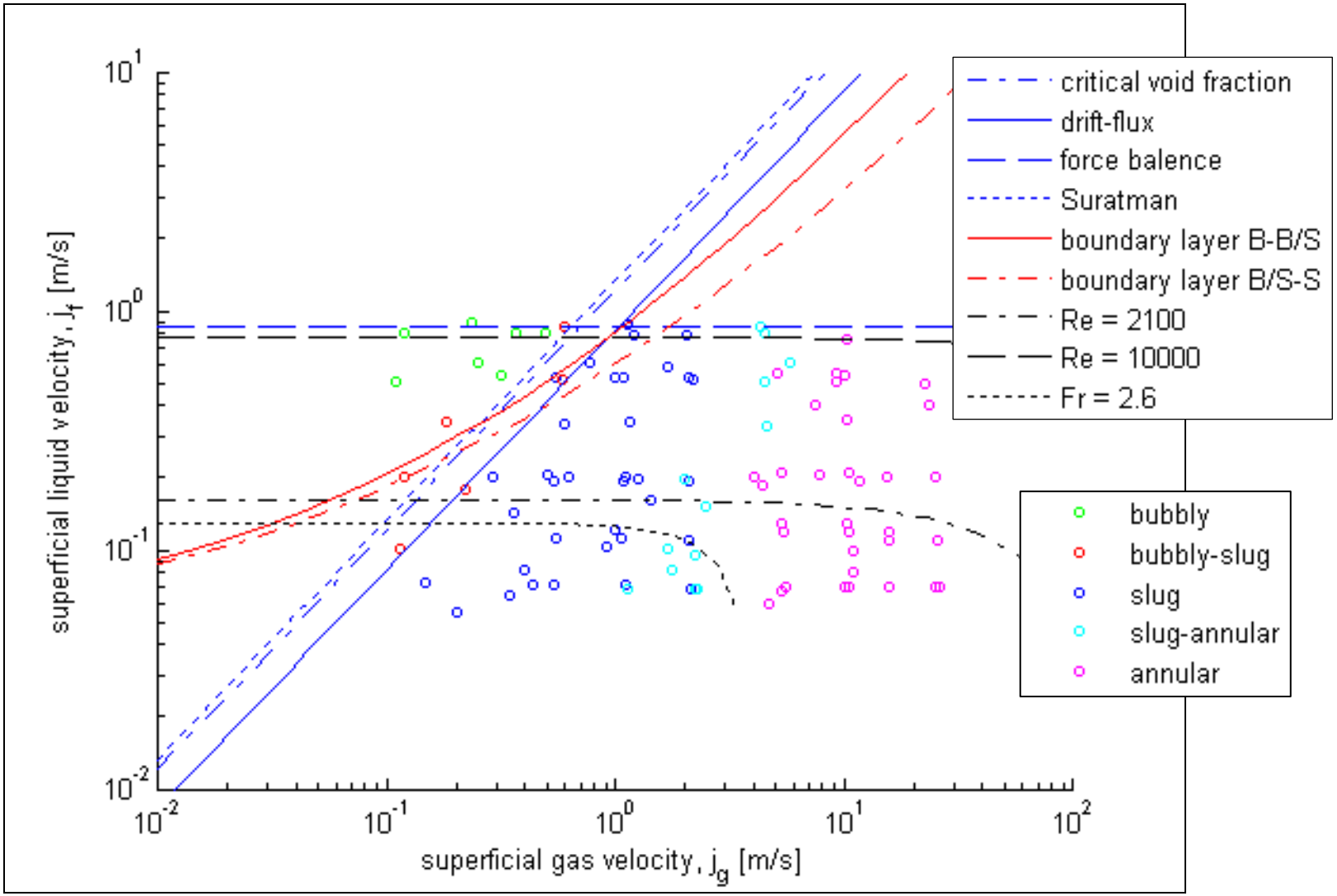

Figure 35 – Bousman (1994) 0.0127 m diameter air-water data set with models.

The force balance model is expected to best represent the slug-to-bubbly/slug transition (not the bubbly/slug-to-slug transition). The mechanisms by which a bubble is disassembled is very different than the mechanisms by which it is assembled. Bubbles can only be taken apart by forces larger than the surface tension forces that hold bubbles together. Because the transitions in the data are not known to be slug-to-bubbly/slug transitions, this model does not apply and it is of no surprise that it does not model the transitions.

The boundary layer models proposed in this study consider both the bubbly-bubbly/slug and bubbly/slug-slug transitions. The boundary layer bubbly-bubbly/slug model successfully defines the transition of all the zero-g qualified data sets. The boundary layer bubbly/slug-slug model is successful in defining the transition for the three Colin and Fabre (1995) data sets but is not consistent with the Bousman (1994) data set. The Dukler et al. (1988) data set does not include enough data points in the bubbly/slug region to be definite but is consistent.

Two data points in the Bousman (1994) data set are significantly outside the explanation of the boundary layer model. The differences in the anatomy of the bubbly/slug-slug transition for the Colin and Fabre (1995) and the Bousman (1994) data sets are speculated to result from differences in mixing apparatus and inlet bubble size distributions. The major difference in the mixing apparatus is that for the Colin and Fabre (1995) experiments, air is injected into a liquid stream while for the Bousman (1994) experiments, liquid is injected liquid into an air stream. There is no further information in the literature which describes the Bousman (1994) and Dukler et al. (1988) mixing apparatus.

The accuracy of the boundary layer models is excellent and clearly models the trends in the data. The precision is less clear and cannot be meaningfully evaluated without a known precision for the data sets.

7.4 SUMMARY

The boundary layer models are successful in defining the bubbly-bubbly/slug and bubbly/slug-slug transitions for the Colin and Fabre (1995) data sets but did not adequately explain the Bousman (1994) data set. The Dukler et al. (1988) data set was irresolute in evaluating the models. The critical void fraction, drift flux, Suratman, and force balance models are inadequate for modeling the bubbly-slug transition.

A major difference exists in the anatomy of the data sets produced by Colin and Fabre (1995) and Bousman (1994). The data sets are anatomically different because of the differences in the mixing apparatus used to produce them. The Colin and Fabre (1995) experiments used a Venturi mixer while the Bousman (1994) experiments used an annular mixer. The major difference between the two types of mixing apparatus is that the Venturi mixer injects air into a water stream while the annular mixer injects water into an air stream. Such a difference is expected to effect the inlet bubble size distribution as well as coalescence.

CHAPTER VIII
CONCLUSIONS AND RECOMMENDATIONS

8.1 CONCLUSIONS

8.1.1 ZERO-G QUALIFICATION OF DATA SETS

A set of criteria was developed to determine if a data set was representative of zero-g or exhibited undue buoyancy effects. Coalescence was shown to be promoted by buoyancy, which in turn is caused by residual acceleration. These buoyancy effects caused a measurable change in the critical void fraction at which transitions occur.

The zero-g quality criteria require tri-axial accelerometry, buoyancy forces to be an order of magnitude less than surface tension and inertial forces, and adequate flow development length and time. When data sets that did not pass the zero-g quality criteria were compared with data sets that did, the degree by which buoyancy effects affected the flow regime transitions was apparent.

8.1.2 MICROGRAVITY FLOW PHENOMENON

Boundary layer theory plays an important role in the bubbly-bubbly/slug and bubbly/slug-slug transitions. The laminar sublayer acts as a shear force barrier that keeps bubbles within the center turbulent channel. The laminar sublayer approximates the point where the viscous forces become greater than the surface tension forces. Bubbles larger in diameter than the center turbulent channel elongate instead of extending in to the laminar sublayer.

The critical void fraction was previously thought to be an empirical constant which defined the bubbly-slug transition. This study demonstrates that the critical void fraction

is not an empirical constant but instead a physical parameter which describes critical bubble packing. Critical packing is a function of the laminar sublayer thickness. Critical bubble packing causes bubbles to meet and coalesce. When some bubbles diameters become larger than the center channel, the bubbly-bubbly/slug transition occurs. When all bubbles become larger than the center channel, the bubbly/slug-slug transition occurs.

Because the flow regime transitions are dependent on the inlet bubble size distribution, the flow regime transitions are specific to the type of mixing apparatus used in the experiment. Thus, the anatomy of the flow regime maps differs for each type of mixing apparatus. Fine control of the inlet bubble size distribution leads to very predictable bubble coalescence along the development length. Loose control of the inlet bubble size distribution leads to less predictable bubble coalescence.

8.1.3 BUBBLY-BUBBLY/SLUG AND BUBBLY/SLUG-SLUG TRANSITION MODELING

The new models presented in the study are entirely physical, dimensionless, and easy to use. The new boundary layer models for the bubbly-bubbly/slug and bubbly/slug-slug transitions are demonstrated to be very successful. Other models in the literature do not adequately approximate the bubbly-slug transition, nor account for the presence of the bubbly/slug regime.

The laminar sublayer thickness and critical void fraction can be expressed as functions of the Reynolds number. The boundary layer models can be expressed as a function of the Reynolds number and flow rates.

One-g single-phase pressure drop, wall shear, and friction factor models are good approximations for modeling zero-g two-phase flow.

8.2 RECOMMENDATIONS FOR FUTURE WORK

Close examination of coalescence along the development length is needed to fully understand the coalescence affects along the development length. Measurement of bubble diameters and distributions at the inlet and exit of the test section are needed and should be included in all future experiments. Video which follows the development of specific bubbles from inlet to exit would be of extraordinary value.

Further experimentation with mixing apparatus, inlet bubble size distribution, and the resulting effect on flow regime is needed. Also of value is the ability to control and predict the inlet bubble diameter and distribution. Lastly, the upper limit on the critical void fraction a mixing apparatus can produce should also be acknowledged in the study.

The use of one-g two-phase pressure drop, friction factor, and wall shear models to approximate zero-g two-phase flow near the wall should continue to be evaluated.

The quality and resolution of experimental data sets are improving but further improvements are needed.

The quality criteria used to determine if a data set is representative of zero-g flow should continue to be improved.

REFERENCES

Bousman, W.S., 1994. Studies of two-phase gas-liquid flow in microgravity, Ph.D. dissertation., University of Houston.

Colin, C., 1990. Ecoulements diphasiques a bulles et a poches en micropesanteur. M.S. thesis, Institut de Mecaniques des Fluides de Toulouse, France.

Colin, C., Fabre, J., Dukler, A.E., 1991. Gas-liquid flow at microgravity conditions – I. Dispersed bubble and slug flow. Int. J. Multiphase Flow 17, 533-544.

Colin, C., Fabre, J., 1995. Gas-liquid pipe flow under microgravity conditions: influence of tube diameter on flow patterns and pressure drops. Adv. Space Res. 16, 137-142.

Colin, C., Fabre, J., McQuillen, J., 1996. Bubble and slug flow at microgravity conditions: state of knowledge and open questions. Chem. Eng. Comm. 141-142, 155-173.

Dukler, A.E., Fabre, J.A., McQuillen, J.B., Vernon, R., 1988. Gas-liquid flow at microgravity conditions: flow patterns and their transitions. Int. J. Multiphase Flow 14, 389-400.

Ghrist, M.R., 2008. Zero gravity two-phase flow regime transition modeling compared with data and RELAP5-3D predictions. M.S. thesis, Texas A&M University.

Heppner, N.B., King, C.N., Littles, J. W., 1975. Zero-g experiments in two-phase fluid flow regimes. ASME 75-ENAs-24.

Huckerby, C.S., Rezkallah, K.S., 1992. Flow pattern observations in two-phase gas-liquid flow in a straight tube under normal and microgravity conditions. AIChE Proc. 88, 139-147.

Janicot, A.J.P., 1998. Experimental and theoretical studies of gas-liquid two-phase flow at reduced gravity conditions. M.S. thesis, University of Houston.

Jayawardena, S.S., Balakotaiah, V., Witte, L.C., 1997. Flow pattern transition maps for microgravity two-phase flows. AIChE J. 43, 1637-1640.

Lin, C.S., Moulton, R.W., Putnam, G.L., 1953. Mass transfer between solid wall and fluid streams. Ind. Eng. Chem. 45, 636-640.

Lovell, T.W., 1985. Liquid-vapor flow regime transitions for use in design of heat transfer loops in spacecraft: an investigation of two phase flow in zero gravity conditions. Air Force Wright Aeronautical Laboratories Technical Report, AFWAL TR-85-3021.

Reinarts, T.R., 1993. Adiabatic two-phase flow regime data and modeling for zero and reduced (horizontal flow) acceleration fields. Ph.D. dissertation, Texas A&M University.

Zhao, L., Rezkallah, K.S., 1993. Gas-liquid flow patterns at microgravity conditions. Int. J. Multiphase Flow 19, 751-763.

Zhao, J.F., Xie, J.C., Lin, H., Hu, W.R., Ivanov, A.V., Belyaev, A.Y., 2001. Experimental studies on two-phase flow patterns aboard the Mir space station. Int. J. Multiphase Flow 27, 1931-1944.

Zuber, N., Findlay, J.A., 1965. Average volumetric concentration in two phase flow systems. J. Heat Transfer 87, 453-468.

VITA

Name: Adam Michael Shephard

Address: Texas A&M University
Department of Nuclear Engineering
3133 TAMU
College Station, TX 77843-3133

Email Address: shephard@tamu.edu

Education: M.S., Nuclear Engineering, Texas A&M University, 2009
B.S., Industrial Engineering, Texas A&M University, 2005